

Toward Electrically Pumped Organic Lasers: A Review and Outlook on Material Developments and Resonator Architectures

Qi Zhang, Wenwen Tao, Jingsong Huang, Ruidong Xia,*
and Juan Cabanillas-Gonzalez*

Organic lasers have undergone decades of development. A myriad of materials with excellent optical gain properties, including small molecules, dendrimers, and polymers, have been demonstrated. Various resonator geometries have also been applied. While sharing the advantages of the solution processability and mechanical flexibility features of organic materials, organic optical gain media also offer interesting optical properties, such as emission tunability through chemical functionalization and inherent large optical gain coefficients. They offer prospects for different applications in the fields of bioimaging, medicine, chemo- and biosensing, anticounterfeit applications, or displays. However, the realization of electrically pumped organic lasers still remains a challenge due to the inherent drawbacks of organic semiconductors, e.g., modest carrier mobility, long-lived excited-state absorption, and extra losses which originate in the device (e.g., absorption from metal electrodes). Herein, the past developments of organic lasers are discussed, highlighting the importance of materials and cavities with regard to the goal of electrically pumped organic lasers. The latest progress and the possible ways to address the challenge are discussed.


the stimulated emission (SE) phenomenon in 1917. It laid the foundation of various applications in scientific research, industrial manufacture, and in our daily life. The first laser device was demonstrated using a ruby crystal as optical gain medium in 1960.^[1] Following this first demonstration, lasers based on crystals, gases, organic dyes, and solid-state semiconductors as optical gain media sprang up within a decade, boosting the development of the field. The first solid-state dye laser reported in 1967 was based on Rhodamine 6G embedded in polymethylmethacrylate (PMMA). PMMA worked as a solid-state matrix to prevent dye aggregation and fluorescence quenching.^[2] Another important milestone was the observation of laser action in organic crystals, demonstrated in anthracene-doped fluorene single crystals with violet laser emission in 1972.^[3] A few years later, triggered by the developments of organic light-emitting diodes (OLEDs),^[4] the first optically pumped polymer laser was realized based on poly[2-methoxy-5-(2-ethylhexyloxy)-1,4-phenylenevinylene] (MEH-PPV).^[5] Ever since this milestone

1. Introduction

Laser was one of the most important inventions in the 20th century as an outgrowth of Albert Einstein's prediction of

Dr. Q. Zhang, Prof. R. Xia
Key Laboratory for Organic Electronics and Information Displays (KLOEID)
Institute of Advanced Materials (IAM)
Jiangsu National Synergetic Innovation Center for Advanced Materials (SICAM)
Nanjing University of Posts & Telecommunications
9 Wenyuan Road, Nanjing 210023, P. R. China
E-mail: iamrdxia@njupt.edu.cn

Dr. Q. Zhang
Physical Science and Engineering Division (PSE)
King Abdullah University of Science and Technology (KAUST)
Thuwal 23955-6900, Saudi Arabia

 The ORCID identification number(s) for the author(s) of this article can be found under <https://doi.org/10.1002/adpr.202000155>.

© 2021 The Authors. Advanced Photonics Research published by Wiley-VCH GmbH. This is an open access article under the terms of the Creative Commons Attribution License, which permits use, distribution and reproduction in any medium, provided the original work is properly cited.

DOI: 10.1002/adpr.202000155

W. Tao, Dr. J. Huang
Oxford Suzhou Centre for Advanced Research (OSCAR)
University of Oxford
Suzhou 215123, P. R. China

Prof. R. Xia
The International School of Advanced Materials
School of Material Science and Engineering
South China University of Technology
381 Wushan Road, Tianhe District, Guangzhou 510640, P. R. China

Dr. J. Cabanillas-Gonzalez
Madrid Institute for Advanced Studies
IMDEA Nanoscience
Ciudad Universitaria de Cantoblanco
Calle Faraday 9, Madrid 28049, Spain
E-mail: juan.cabanillas@imdea.org

was achieved, several lasers based on films from different conjugated polymers were reported.^[6]

The development of organic solid-state lasers (OSLs) stalled in the recent years despite the extensive portfolio of organic-based compounds with optical gain properties being reported. This was due to the uncertain prospects of achieving electrically pumped organic lasers. Indeed, optical pumping by primary light sources seemed to be the only feasible operation principle until recently. Electrically pumped lasing appeared out of reach due to the inherent limitations of organic semiconductors, restricting the potential applications of OSLs to a few niche markets. To bypass the difficulties of achieving lasing through electrical pumping, organic laser pumping by compact inorganic light sources such as laser diodes (LDs) or light-emitting diodes (LEDs) has been proposed.^[7–9] This goal was finally realized because of the increase in output power of inorganic LDs/LEDs and the decrease in lasing threshold of organic lasers. The added value of combining an organic laser with an inorganic light as pumping source is the possibility of achieving large spectral tunability, which is provided by the organic gain medium.^[7a] Yet, despite this achievement, the development of electrically pumped organic lasers still remains of major interest in the organic optoelectronics field. Some recent studies have demonstrated evidences that the inherent properties of organic semiconductors, which limited the achievement of organic LDs, could be circumvented.^[10] Nevertheless, a considerable number of scientists have expressed their reservations in view of the complexity of the problem and the technological challenge involved in material synthesis and device configuration.^[11,12]

Very recent progress which stems from intensive materials screening and an increasingly complex laser cavity configuration has been put forward, opening new prospects and expectations in the field. In this Review, we will discuss both the material and device developments in the field together with the most important issues, which, we believe, have so far prevented the realization of organic LDs. This article is organized with the following structure: the photophysics of the organic semiconductors is first described to assist visualizing the main

limitations regarding the development of organic LDs. Second, issues related to failure in electrically pumped organic lasers will be addressed. Third, representative materials, including the most promising approaches for organic LDs, will be reviewed. Fourth, several organic laser cavities and their processing methods will be outlined. Finally, we will share our viewpoints on future developments of organic lasers.

2. Fundamental Photophysics of Organic Gain Medium

When enumerating the key optical properties of organic semiconductors, strong absorption and efficient luminescence are often mentioned. The typical absorption cross-section (σ_{abs}) value for π -conjugated molecules and polymers is in the order of 10^{-16} cm^2 . This value guarantees 90% light absorption for film thickness in the 100 nm range, which brings two major benefits. First, it constitutes a strong asset for optical-pumping operation as it allows the achievement of population inversion at low pumping fluences in films.^[6b] Second, the SE cross section (σ_{SE}) is considered to be correlated with the absorption cross section (σ_{abs}), enabling high optical gain.^[13] Broad fluorescence spectra allow, on the other hand, for broadband amplification.^[14,15] In addition, the photoluminescence (PL) spectra can be tailored by backbone modification, e.g., by controlling the conjugation length^[16] or by the introduction of electron-donor or electron-acceptor groups,^[17] in contrast to inorganic semiconductors where the emitting wavelengths are restricted to lattice-matching requirements. The efficiency of solid-state light emission is quantified through the photoluminescence quantum efficiency (PLQE), which stands for the ratio between the number of emitted and absorbed photons.^[18] Considerable efforts have been devoted to further increase the PLQE of organic semiconductor thin films to achieve high gain and low-threshold organic lasers.^[14a,19] The major strategy to achieve this goal is to localize excitons and minimize the intermolecular interactions, so that dynamic and static luminescence quenching is reduced.^[20] Organic

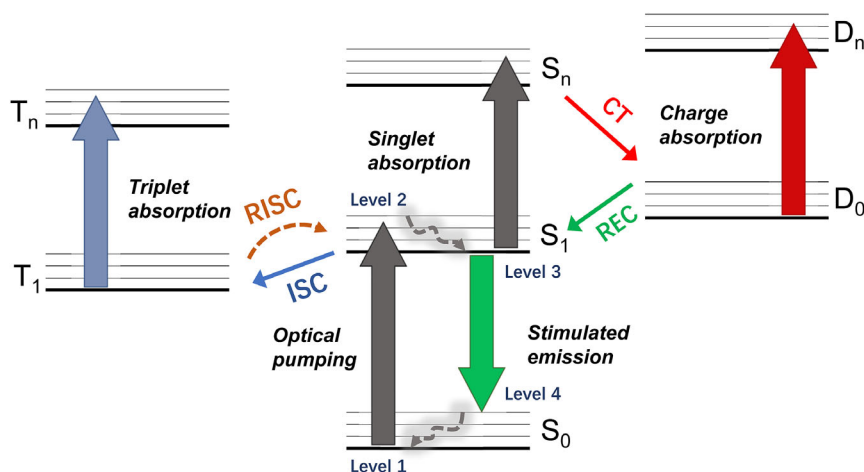


Figure 1. Energy-level diagram of an organic semiconductor: singlets, triplets, and charges. Levels 1–4 labeled in the figure demonstrate the four-level system in the organic gain medium. ISC, RISC, CT, and REC in the figure mean intersystem crossing, reverse intersystem crossing, charge separation, and carrier recombination, respectively.

semiconductors behave as four-level laser systems (**Figure 1**). The absorption of an incident photon promotes an electron from the ground state (S_0) to high-lying electronic states (S_n) followed by subpicosecond internal conversion to the lowest-electronic excited-state (S_1) vibrational manifold.^[21] As the spacing between the different vibronic sublevels is 0.1–0.2 eV, very fast relaxation (picosecond range) to the lowest vibrational level occurs. Thus, efficient population inversion takes place between the lowest vibrational level of S_1 and the higher unoccupied vibrational levels of S_0 manifold. Ground-state recovery is then completed via ground-state thermalization. This four-level configuration permits laser action at very low pumping rates.

While singlet excited states contribute to optical gain, other excited states such as triplets and polarons are regarded as detrimental for lasing. Triplet levels (T_n) are commonly populated by intersystem crossing from the singlet manifold, the lowest triplet level (T_1) being located below S_1 .^[22] Triplets have typically longer decay lifetime^[23] compared with singlet excited states. The absorption ascribed to T_1 – T_n displays characteristic long tails, which often extend up to the SE spectral region.^[24] Triplets are a major obstacle for the development of organic LDs as they are the major products of charge recombination.^[25] Polarons are regarded as charged states that are deemed to form through charge localization into the organic layer either through charge injection or through dissociation of neutral singlet or triplet states. The polaron absorption band usually covers a broad visible spectra range,^[26] which leads to persistent harm over optical gain and lasing action. It is noteworthy that polarons can migrate between separated molecules or along conjugated polymer chains.^[19b,c,27] Two geminate polarons located on the same chain have a large probability of coalescence and, therefore, have shorter lifetime, and are less harmful for optical gain. However, geminate polarons located on different chains show a more persistent detrimental effect over optical gain.^[19c]

3. Key Issues Faced by Electrically Pumped Organic Lasers

Lasing under electrical pumping is the ultimate goal and the strongest motivation for researchers involved in the field of organic lasers. As we mentioned above, there are several issues related to failure in electrically pumped organic lasers. The key drawbacks of materials are low carrier mobility, long-lived/broad absorption from triplets and polarons, and environmental or thermal stability problems of the organic gain layer. There are also issues regarding device design, such as absorption losses arising from the electrodes and heat accumulation.

3.1. Triplets

In general, triplets do not contribute to lasing due to the long timescales associated with intersystem crossing and population of T_1 levels.^[28] Triplet absorption is however one of the key optical losses for lasing, on account of the large T_1 – T_n absorption cross-section values (in the order of 10^{-16} cm²)^[29] and long absorption tails.^[30] The T_1 decay lifetime is in the microsecond–millisecond range.^[31] Therefore, when it comes to optical pumping, photoexcitation with short pulses (<10 ns) and low

repetition rate (<1 MHz) helps minimize triplet absorption losses.^[32] Nonetheless, it is difficult to circumvent triplet absorption in electrically pumped lasers due to the limited modulation frequency of organic LDs and the 1:3 singlet-triplet formation ratio, which results from charge recombination. In addition to triplet absorption, singlet-triplet annihilation is another limiting factor, which becomes more important as the optical pulse length or the pumping frequency increases. To overcome the problem of triplet accumulation, different strategies have been proposed, including the use of materials with very low intersystem-crossing rates, organic compounds in which triplet absorption do not overlap with SE,^[10,33] or thermally activated delayed fluorescence (TADF) materials.^[34] In a recent study, Adachi and coworkers exploited blends from a triplet scavenging host and a guest dye laser to effectively neutralize singlet-triplet quenching. This strategy requires selecting suitable hosts bearing a T_1 level below the guest T_1 level. In this work, this was achieved by synthesizing a novel laser dye with low S–T energy offset. This combination led to the observation of continuous-wave (CW)-pumped lasing.^[33b] In another recent work, Mai et al. reported the use of a novel conjugated host composed of *N,N*-dicarbazolyl-3,5-benzene with a cyclooctatetraene triplet scavenger moiety linked via a nonconjugated bridge, confirming the complete suppression of singlet-triplet annihilation both in films and in OLEDs.^[35]

3.2. Polarons

Polaron absorption associated with charge localization in organic semiconductors also leads to optical losses. Polarons typically exhibit broad absorption bands which overlap with SE bands in some cases. Similar to triplets, polarons can also promote singlet quenching through annihilation processes.^[26a] In an organic LD, the intrinsic low carrier mobility of organics (most are in the range of 10^{-5} – 10^{-2} cm²/(V s), e.g., hole mobility of poly(9,9-dioctylfluorene) is 4×10^{-4} cm²/(V s)),^[36] which implies that the current flow to drive the sandwich-type device has to be very high to sweep away carriers from the optical gain region. In an earlier report, an optically pumped distributed feedback (DFB) laser based on a green-emitting oxetane-functionalized poly(spirobifluorene) integrated in a functional OLED structure exhibited a 15% increase in threshold (from 4.8 to 5.6 μJ cm⁻²) when driven at a low current density of 7 mA cm⁻².

3.3. Stability

Environmental stability and heat management are two problems that must be taken into account in electrically driven diodes. In inorganic lasers, a typical operating current density is 1 kA cm⁻². For comparison, in an organic sandwich-type structure, the estimation of minimum current density to reach the lasing threshold is ≈ 100 A cm⁻².^[12b,37] Typical OLED devices are usually driven under much smaller current densities in the range of 0.01 A cm⁻²,^[38] yet current densities of the order kA cm⁻² or 100 kA cm⁻² can be reached in OLEDs^[39a] and in light-emitting field-effect transistors (LEFETs), respectively.^[39b,c] Considering the extra losses mentioned above, the current density needed to achieve net gain can easily exceed this value. Under these

circumstances, heat accumulates quickly in devices as organics are normally poor thermal conductors. It has been reported that conjugated polymers such as poly(9,9-dioctylfluorene-*co*-benzothiadiazole) (F8BT) undergo crystallization and lose their lasing properties when exposed to high temperatures.^[40] It is thus expected that under high current injection, degradation effects triggered by poor heatsinking and thermal stability may cause short operation lifetimes of the devices. Small molecules and dendrimers are regarded to have better environmental stability,^[41] although they do not always offer the advantages of polymers in terms of solution processability. In addition, the synthesis of dendrimers is complex, which limits their potential applications. To partly address the heat management problem, one can replace the commonly used quartz or glass substrate by other substrates with higher thermal conductivity such as sapphire.^[42]

3.4. Electrodes

Electrodes must be integrated in the device geometry to achieve sufficient current injection. Although polymer electrodes have previously been implemented,^[43] metallic electrodes are still widely applied in organic optoelectronics. Unfortunately, electrodes generally have large absorption coefficients in a wide spectral range overlapping with the emission from organic luminophores. Electrode loss, therefore, leads to a significant increase in lasing threshold for organic lasers in a device structure.^[44] The interaction between the resonating mode and metal absorption also causes a reduction in the *Q*-factor. Planar geometries such as those of LEFETs may bring relief from this problem due to the increase in distance between the electrodes and the charge recombination zone.

3.5. Fabrication of Feedback Structures

An important element to be taken into account is the integration of the feedback structure in the electrically pumped device. Different feedback resonators have been applied in optically pumped organic lasers to implement a feedback loop. In general, the geometry and physics of resonators are similar for organic and inorganic lasers. The oscillator geometry defines the allowed resonant frequencies and the spatial characteristics of the output laser. In our opinion, 1D or 2D DFB gratings have proved to be the most versatile resonator geometry for thin-film organic lasers due to their easy implementation on the organic gain layer or an interface layer in an OLED/LEFET configuration.^[10,45] In optically pumped DFB organic lasers, the gain medium is usually spin coated directly onto prepatterned silica substrates. This is, however, not the case for electrical-pumped devices, in which the optical gain layer must be sandwiched between electrodes and transport layers in a multilayer structure. The main problem here is how to transfer the DFB cavity structure into the device without excessive interference with the device operation conditions. Soft imprint lithography can be an attractive way to realize diffractive patterns on interfacial layers or in the organic gain medium itself.^[46]

Another possible geometry could be a Fabry–Perot microcavity formed by depositing organic gain medium in a sandwich structure between two sets of mirrors.^[47] Liu et al.^[48] reported

extremely low-threshold lasing action from 4-(dicyanomethylene)-2-*i*-propyl-6-(1,1,7,7-tetramethyljulolidyl-9-enyl)-4H-pyran-doped tris(8-hydroxyquinoline) aluminum (Alq₃) film in a high-*Q* microcavity structure. The difficulty with this design is the insertion of the electrodes. Other resonator structures, such as whispering gallery-mode (WGM) resonators and random lasers, have also been used to achieve high *Q*-factor and low-loss optically pumped organic lasers. The preparation process for both random laser and WGM resonators is relatively simple and suitable for solution-processed organic device technology, offering the potential to be integrated into electrically pumped devices. However, the integration process of the feedback structures in an electrically pumped device configuration still has to be developed.

3.6. Lasing Oscillation Under the Long-Pulse Photon Excitation Regime

The realization of electrically pumped organic lasers is a complex task relying on the development of new gain materials and carefully designed cavities. The materials are expected to possess numerous properties, such as high gain, high and balanced carrier mobilities, minimized population of slow decay species, and good thermal stability. Concerning laser cavity design, consideration must be given to the electrode arrangement, enabling effective current injection and avoiding extra losses and some other issues. For these reasons, it is worth mentioning that some laser operation schemes have been alternatively explored, such as CW optical pumping, in which the electrode-related issues do not have to be addressed.^[33,49,50] CW optically pumped lasers are not only a breakthrough in themselves, but they also pave the way for the final realization of electrically pumped organic lasers. Similar to electrically pumped lasing, slow decaying species such as triplets or polarons must be dissipated properly to avoid harmful spectral overlap with SE.^[12a] Some efforts have been already done in this direction. Mróz et al.^[49d] reported quasi-CW amplified spontaneous emission (ASE) in a green-emitting-conjugated polyrotaxane (Rtx), where absorption from long-lived polaronic states was hindered due to the supramolecular encapsulation of the polymer backbone by cyclodextrin rings. Adachi and coworkers^[33a] reported the realization of a quasi-CW optically pumped organic laser operating under two different pumping schemes: with 10 ps pulses at a repetition rate of 80 MHz and with 30 ms pulses at > 16 KHz repetition rate (see in **Figure 2**). The organic gain layer was based on 4,4'-bis[(*N*-carbazole)styryl] biphenyl (BSB-Cz), which exhibited very-low triplet formation yield and negligible triplet absorption in the spectral range of SE. In a more recent report,^[33c] this principle was extended to a novel solution-processable laser dye, bis(*N*-carbazolylstyryl)-9,9-dihexylfluorene (BSFCz). By blending it with a wide-bandgap host, tris(4-carbazoyl-9-ylphenyl)amine (TCTA), quasi-CW lasing action at long-pulse excitation (10 ms) was achieved in second-order DFB gratings.

4. Material Developments and Strategies to Overcome the Problems

The road toward electrically pumped organic lasers goes through the implementation of novel materials with improved properties.

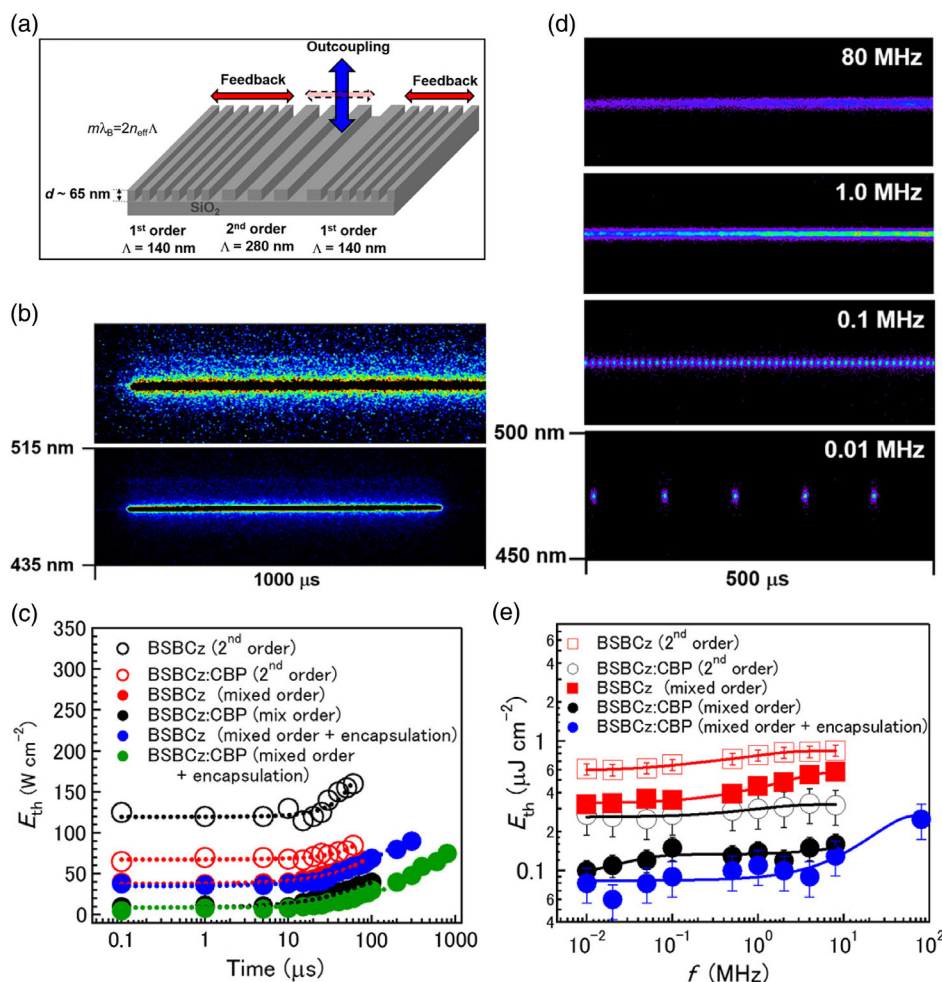


Figure 2. Quasi-CW optically pumped organic laser. a) Schematic representation of the mixed-order DFB grating structure used. b) Streak camera images of laser emission integrated from a BSBCz:CBP (20:80 wt%) film on mixed-order DFB under the pumping pulses of 30 ms and 2.0 kW cm⁻² (top) or 800 μs and 200 W cm⁻² (bottom) over 100 pulses. c) Lasing threshold versus pump pulse duration in various DFB devices. d) Streak camera images of laser oscillations from BSBCz:CBP layer on mixed-order DFB at different repetition rates from 0.01 to 80 MHz over a period of 500 μs. e) Lasing threshold versus repetition rate in different DFB devices. Reproduced with permission.^[33a] Copyright 2017, American Association for the Advancement of Science.

Organic gain materials branch into several different families. In general, they all share a common π -conjugated nature containing multiple luminophores, in many cases, functionalized with side groups, to enhance solution processability. They can be classified, according to their molecular weight, into small molecules (<1000 Da, see in **Figure 3** for the chemical structures of typical small molecules), dendrimers (also known as star-shaped compounds) which comprise a core covalently linked to several arms (up to 10 kDa, see in **Figure 4**, for the chemical structures of typical dendrimers), and linear polymers with several hundreds of repeat units (up to 100 kDa, see in **Figure 5** for the chemical structures of typical polymers).

Dye molecules generally show often a tendency to crystallize in solid state and form nonemissive aggregates, which are unfavorable to their optical gain properties. Their functionalization with bulky and steric side groups can partly hinder π -stacking and enable excellent film-formation properties.^[51] A different category consists of molecules that have the tendency to arrange into luminescent single crystals with well-defined geometries.

Properly designed crystals can combine excellent luminescent properties with high charge mobilities,^[52] becoming very attractive candidates for OLEDs or electrically pumped lasers. The advantage of small molecules is their high purity and structural definition, leading to stable and predictable properties.

Dendrimers share with small molecules their well-defined structural properties. The long-conjugated arms attached to the core provide a way to tune the electronic properties while promoting steric hindrance to suppress luminescence self-quenching in the solid phase. However, the synthesis of dendrimers typically involves complex routes including multiple coupling reactions and purification steps which are costly and time-consuming. An additional drawback is their poor solubility and modest film-forming ability.

Polymers, on the other hand, exhibit large solubility and film-forming properties, which make them compatible with solution-processable methods for large-area deposition such as inkjet printing or spray coating compatible with roll-to-roll fabrication.

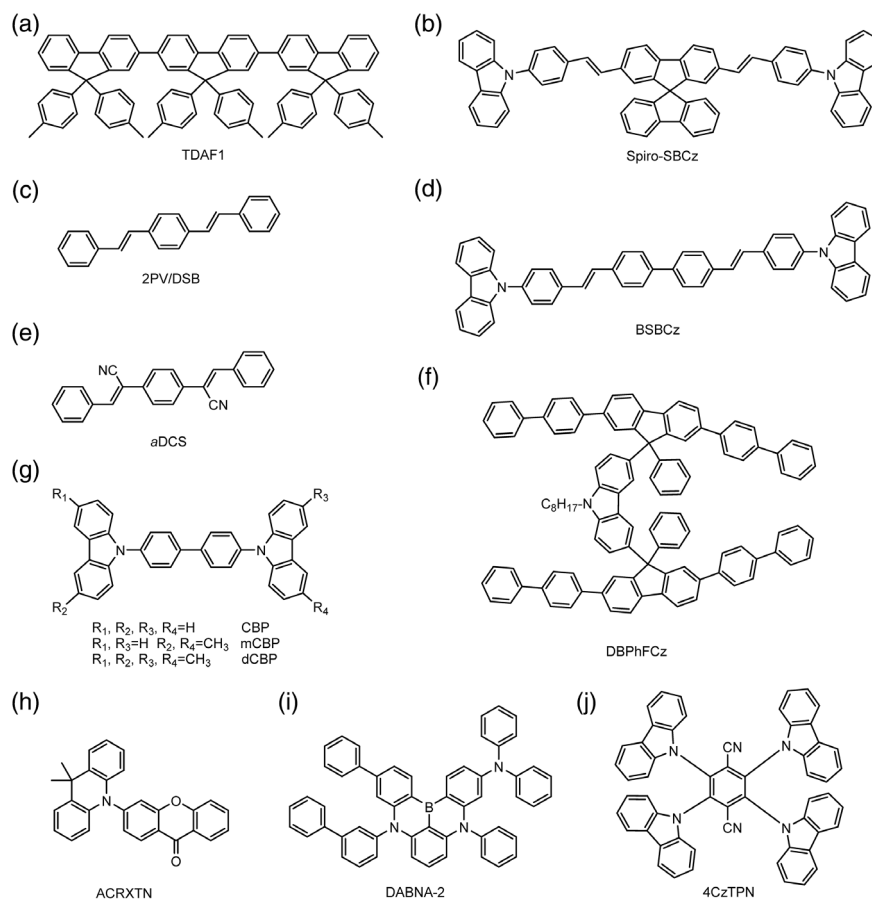


Figure 3. Chemical structures of typical small molecules: a) adapted from Oyamada et al.,^[58] b) Nakanotani et al.,^[63] c) Wang et al.,^[69] d) Aimono et al.,^[77] e) Yoon et al.,^[70a] f) Zhang et al.,^[40] g) Aimono et al.,^[77] and Nakanotani et al., Zhao et al., and Ye et al., and,^[34a,b,d] h) Nakanotani et al.,^[34a] i) from Zhao et al.,^[34b] and (j) Zhao et al.^[34c]

However, polymers have polydispersity and their purification is harder to control. Defect sites on the polymer chains or catalytical residuals cannot be completely avoided through a typical purification process, i.e., precipitation and extraction. As a result, the photophysical properties of polymers are highly dependent on the degree of disorder, molecular weight, and polydispersity.

The large library of organic laser compounds reported in the past years has recently been applied to predict the optoelectronic properties of novel designed compounds. Ou et al., for instance, reported on a computational screen-out strategy assisted with density functional theory (DFT) and time-dependent DFT (TDDFT) to predict the light amplification performance and then the possibility for realizing electrically pumped organic lasers.^[53] However, these methods are restricted to small molecules due to their relative simplicity and well-defined structure. In this section, we will briefly review the typical families of organic semiconductors, highlighting those that appear relevant for the development of electrically pumped lasers. It is important to notice that hereafter charge transport properties will be often referred in concomitance to lasing properties due to their relevance for OLEDs and electrically pumped lasers.

4.1. Small Molecules

4.1.1. Fluorene-Based Molecules

Fluorene is a well-developed molecule which can be functionalized with halides, facilitating cross-coupling reactions to form macromolecules. Usually, alkyl chains are used for substitution in the 9,9'-position for enhancing solubility. The ASE behavior of hexyl-substituted oligofluorenes, namely, terfluorene, pentafluorene, heptafluorene, and octafluorene, was already demonstrated.^[54] Upon thermal annealing, the hole field-effect mobility showed two orders of magnitude increase in pentafluorene. However, substitution with branched side chains leads to poor film-forming ability due to reduced solubility. Some interesting developments have been done with oligofluorene lasers in the liquid phase. Ribierre et al. observed ASE in nonvolatile fluidic fluorene homologues substituted with long branched siloxane groups. A threshold value of $1.4 \mu\text{J cm}^{-2}$ was found with fluorene dimers while the hole mobility was $1.3 \times 10^{-4} \text{V}^{-1} \text{s}^{-1}$, comparable with glassy fluorene films.^[55] By dissolving heptafluorene in liquid ethylhexyl-functionalized carbazole host (EHCz), low-threshold ($2 \mu\text{J cm}^{-2}$) DFB optically pumped lasing action was achieved at a high repetition rate of 4 MHz.^[56]

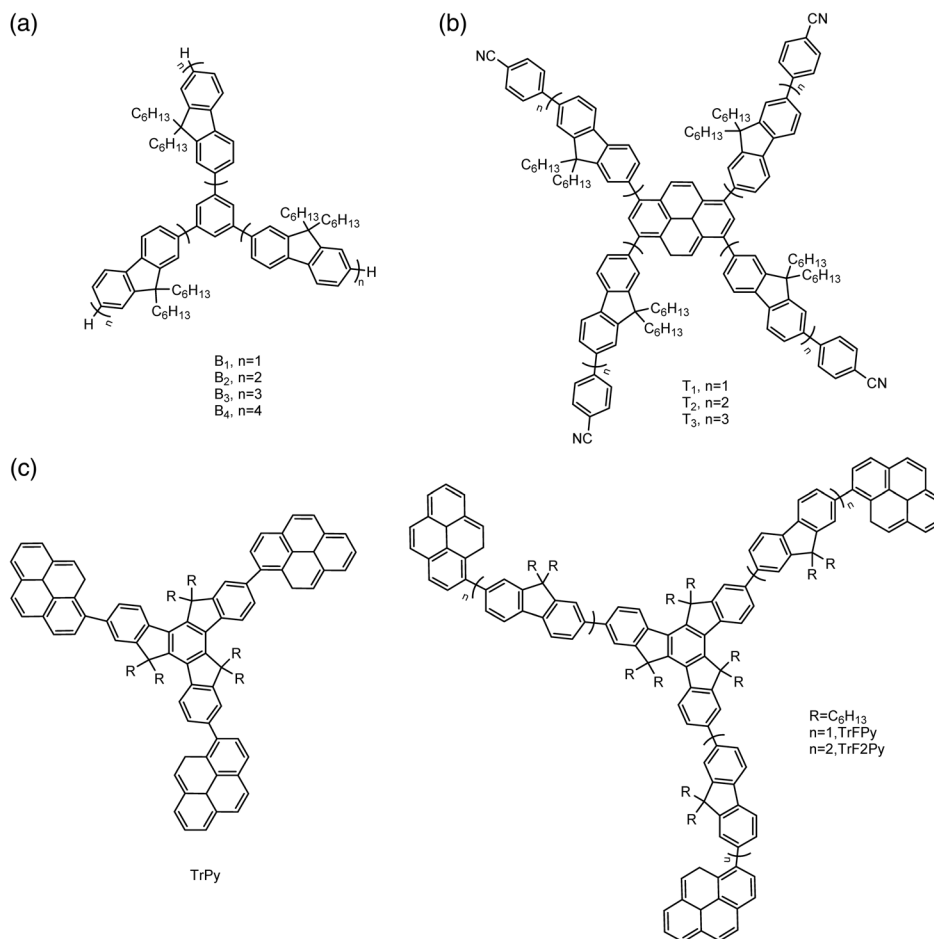


Figure 4. Chemical structures of typical dendrimers: a) comprising a benzene core linked with three oligofluorene arms with various fluorene units (1–4) from the study by Tsiminis et al.,^[81] b) comprising a pyrene core linked with four oligofluorene arms (within fluorene units varied from 1 to 3) capped by cyanophenyl moieties from the study by Zhang et al.,^[41b] c) comprising a truxene core linked with three oligofluorene arms (within fluorene units varied from 0 to 2) capped by pyrene from the study by Xu et al.^[86]

Another interesting series of fluorene derivatives are oligo(9,9-diarylfuorene)s, which were first deployed as emissive layers in OLEDs due to their ambipolar charge transport properties.^[57] Oyamada et al. reported ASE on trimer (dimer) oligo(9,9-diarylfuorene) derivatives, bi(ter)(9,9'-spirobifluorene), bi(ter)(9,9-ditolylfluorene), and 4,5-diazafluorene-incorporated ter(9,9-diarylfuorene).^[58] The trimers in general show better optical properties than dimers, a higher PLQE, and lower ASE pumping thresholds. Hsing-Chieh et al. studied the same compounds and realized continuously tunable (430–447 nm) DFB lasers with ter(9,9-diarylfuorene) by annealing films with various conditions, which trigger the reorientation of molecules.^[59]

Spirobifluorenes^[60] are rigid structures with relatively large steric effects bearing the linkage of two perpendicularly arranged fluorene units. This structure preserves the electronic characters of the individual chromophores and suppresses possible crystallization, exciton quenching, and excimer formation. Spher et al. studied the ASE properties of different spiro-compounds, in which vacuum-deposited spiro-SPO (spiro-junction combined with a sexiphenyl chain and an oxadiazole moiety) thin films

displayed the lowest ASE pumping thresholds ($1 \mu\text{J cm}^{-2}$).^[61] Upon spin coating spiro-terphenyl fluorenes on prepatterned DFB gratings with different period parameters (195–250 nm), a reasonably large tuning range of 32 nm in laser emission wavelength (361.9–393.8 nm) (minimal value: $8.9 \mu\text{J cm}^{-2}$) was achieved at relatively low-threshold conditions.^[62] Spirobifluorenes also exhibit notable electroluminescence characteristics. Nakanotani et al. reported the PL and electroluminescence (EL) characteristics of 9,9'-spirobifluorene derivatives, namely, 2,7-bis(*N*-carbazolyl)-9,9'-spirobifluorene (spiro-Cz) and 2,7-bis[4-(*N*-carbazole) phenylvinyl]-9,9'-spirobifluorene (spiro-SBCz), in pristine films and as dopants in 4,4'-bis(9-carbazole)-2,2'-biphenyl (CBP). In the neat film, spiro-SBCz outperformed spiro-Cz, exhibiting $2.7 \times 10^{-4} \text{ cm}^2 \text{ V}^{-1} \text{ s}^{-1}$ hole mobility measured in p-type FETs as well as ASE pumping thresholds of $0.43 \mu\text{J cm}^{-2}$. This value was significantly lowered down to $0.11 \mu\text{J cm}^{-2}$ when spiro-SBCz was dispersed in CBP in a 6 wt% concentration. More interestingly, in unbiased FETs, the measured ASE threshold was only $2.5 \mu\text{J cm}^{-2}$.^[63] Given that they are also highly stable, these materials could be very attractive to explore electrically pumped lasing.

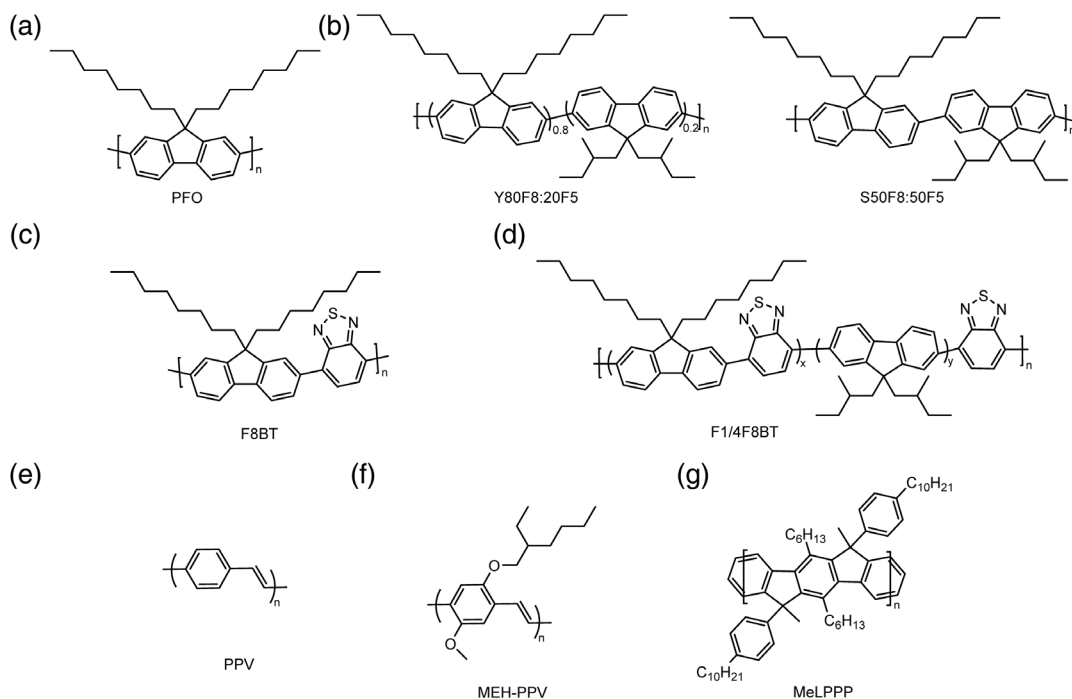


Figure 5. Chemical structures of typical polymers: a) from the study by Xia et al.,^[89] b) Yap et al.,^[19a] c) Xia et al.,^[89] d) Yu et al.,^[94] e) Tessler et al.,^[6b] f) Park et al., and^[98] g) Plumhof et al.^[105]

4.1.2. Styrylbenzene-Based Molecules

Trans-distyrylbenzenes (DSB) are a family of highly relevant crystalline organic laser materials composed of three phenylenevinylene repeat units.^[64] Functionalization of the DSB molecule with different groups in different positions has an enormous impact on the molecular arrangement in the crystalline structure. Kabe et al. reported the effect of the methyl substitution position on intermolecular interactions of the resultant blue-emitting DSB derivatives, i.e., 1,4-bis(2-methylstyryl)benzene (*o*-MSB) and 1,4-bis(4-methylstyryl)benzene (*p*-MSB).^[65] They were found to crystallize in different molecular arrangements due to discrepant molecular conformation caused by the methyl groups. Lower ASE threshold ($\approx 14 \mu\text{J cm}^{-2}$) and faster radiative decay rate were found in *o*-MSB, whereas both *o*-MSB and *p*-MSB exhibited very high PLQE values ($> 88\%$, in the blue emission range). Their radiative decay rate and ASE properties were further promoted upon their dispersion in a conjugated matrix. *p*-MSB exhibited relatively high hole ($\mu_h > 0.1 \text{ cm}^2 \text{ V}^{-1} \text{ s}^{-1}$) and electron ($\mu_e > 0.01 \text{ cm}^2 \text{ V}^{-1} \text{ s}^{-1}$) mobilities in single-crystal organic field effect transistor (OFET) measurements.^[66] Varghese et al.^[67] reported another DSB derivative modified with four methyl substituents on the terminal phenyl groups (4M-DSB), showing a larger optical gain coefficient (77 cm^{-1}) than DSB. Another worth-mentioning substituent is 2,5-diphenyl at 1,4 positions, which gave rise to a cross-stacked crystalline structure with good thermal stability, electroluminescence, and ASE performance ($E_{\text{th}} \approx 680 \mu\text{J cm}^{-2}$).^[68] DSB can also work as a host for tetracene, yielding a high PLQE value of 74% (in the green emission range) and lower ASE threshold ($600 \mu\text{J cm}^{-2}$) compared with DSB.^[69]

DSB derivatives with symmetrical cyanosubstituents, aka DCS, are also efficient fluorophores with rich features in their single crystals. Park and coworkers did a series of studies to understand the origins of the spectral-narrowing phenomenon in such materials.^[70] Varghese et al. identified three different spectral-narrowing mechanisms, ASE, lasing, and stimulated resonance Raman scattering (SRRS) in the single crystal of (2*Z*,2'*Z*)-2,2'-(1,4-phenylene)bis(3-(4-(dibutylamino)phenyl)acrylonitrile) (DBADCS).^[71] In a follow-up work, the single crystal of a similar DCS derivative, (2*Z*,2'*Z*)-3,3'-(1,4-phenylene)bis(2-(4-butoxyphenyl)acrylonitrile) (β -DBDCS), exhibited outstanding emission properties with PLQE of 84%, cavity *Q*-factor of 8700, and threshold of $0.4 \mu\text{J cm}^{-2}$. The lasing modes varied with the excitation-incident direction and depended on the crystal dimensions.^[72] Fu and coworkers reported on organic microlasers based on self-assembled crystals of DSB derivatives, 1,4-dimethoxy-2,5-di[4'-(cyano)styryl]benzene (COPV) and 1,4-dimethoxy-2,5-di[4'-(methylthio)styryl]benzene (TDSB).^[73] Ma and coworkers synthesized and characterized optical gain properties of crystals of highly emissive DSB derivatives, such as cyano-substituted oligo(*p*-phenylene vinylene) (CN-DPDSB),^[74] 1,4-bis(α -cyano-4-diphenylaminostyryl)-2,5-diphenylbenzene (CNDPASDB),^[75] 1,4-bis[1-cyano-2-(4-(diphenylamino)phenyl)vinyl]benzene (TPCNSDB) organic crystals,^[76] and 1,4-bis(2-cyano-2-phenylethenyl)benzene (BCPEB). Good-quality single crystals with a high PLQE value and low ASE/lasing threshold together with balanced ambipolar carrier transport characteristics can be obtained based on these materials. For instance, in single crystals of cyano-substituted oligo(*p*-phenylene vinylene) (CN-DPDSB) grown by physical vapor deposition (PVD), the

balanced hole ($2.5\text{--}5.5 \times 10^{-2} \text{ cm}^2 \text{ V}^{-1} \text{ s}^{-1}$) and electron ($0.9\text{--}1.3 \times 10^{-2} \text{ cm}^2 \text{ V}^{-1} \text{ s}^{-1}$) mobilities were achieved together with low ASE threshold (23 kW cm^{-2}) and high PLQE (95%) in the blue-emission range.^[52e]

4.1.3. Carbazole–Styrylbiphenyl Compounds

The work by Adachi and coworkers on BSB–Cz deserves a special mention here. This compound exhibits unique optical properties when dispersed in a 4,4′-bis(9-carbazolyl)-2,2′-biphenyl (CBP) matrix at 6 wt%, featuring a PLQE of nearly 100%, a radiative decay rate of $1 \times 10^9 \text{ s}^{-1}$, and a very low ASE threshold of $0.32 \mu\text{J cm}^{-2}$ achieved under nanosecond optical pumping at 20 Hz repetition rate.^[77] These record-breaking properties led to the observation of spectral narrowing assigned to ASE upon CW optical pumping with 640 W cm^{-2} power density.^[48b] Interestingly, the same study showed no evidences for any excited-state absorption from singlets or triplets at the wavelength peak of ASE, which was proposed to be the key property. Quasi-CW lasing was demonstrated with a threshold of $0.25 \mu\text{J cm}^{-2}$ on the same optical gain medium in second-order DFBs upon photoexcitation at 365 nm with 10 ps and 8 MHz repetition rates.^[48e] A further improvement was later reported in mixed-order DFBs and improved encapsulation, achieving lasing at the threshold of $0.25 \mu\text{J cm}^{-2}$ upon 80 MHz pump pulse repetition rate. The stability of the device operating under 80 MHz excitation was also enhanced significantly: a 4% of output intensity loss was found after 20 min of operation.^[33] BSB–Cz:CBP is therefore a front-runner candidate for the development of electrically pumped organic lasers.

4.1.4. TADF Materials

The inclusion in the organic gain layer of TADF materials, featuring reverse intersystem crossing (RISC) from triplet to singlet levels, provides a possibility to overcome the problem of triplet absorption in organic lasers. In these materials, the energy offset between S_1 and T_1 is low enough ($<0.1 \text{ eV}$) to trigger T_1 to S_1 thermal conversion at room temperature. A considerable number of reports^[78] on TADF-based OLEDs have been released in recent years following the first success with 4CzIPN.^[79] The very first trial with TADF materials in light amplification involved the use of 3-(9,9-dimethylacridin-10(9H)-yl)-9H-xanthen-9-one (ACRXTN) as a triplet harvester codoped together with 2,3,6,7-tetrahydro-1,1,7,7-tetramethyl-1H,5H,11H-10-(2-benzothiazolyl)quinolizino-[9,9a,1gh] coumarin (C545T) in a 3,3-di(9H-carbazol-9-yl)biphenyl (mCBP) host.^[34a] The resultant ternary blend exhibited superior optical gain and electroluminescence properties with a lower threshold and higher efficiency compared with C4C5T:mCBP without ACRXTN dopant. Bearing in mind these results, Nakanotani et al. reported the direct observation of ASE at a threshold of $1.6 \mu\text{J cm}^{-2}$ in a TADF emitter (9-([1,1′-biphenyl]-3-yl)-N,N,5,11-tetraaryl-5,9-dihydro-5,9-diaza-13b-boranaphtho[3,2,1-de]anthracen-3-amine) (DABNA-2) dispersed in mCBP.^[34b] Ye et al. reported on near-infrared (NIR) ASE from TADF curcuminoid boron difluoride dyes doped in CBP.^[34d] Huang et al. fabricated a microring WGM resonator with a TADF emitter,

4,6-bis((E)-9-ethyl-3-vinyl-9H-carbazole)-5-(ethoxycarbonyl)-2,2-difluoro-2H-1,3,2-dioxaborin-1-ium-2-uide, namely, CAZ-A/CPB, which exhibited a clear laser peak at 683 nm with a threshold value of $3.96 \mu\text{J cm}^{-2}$ and Q factor of ≈ 1300 .^[80] In a very recent work,^[34c] Zhou et al. reported direct evidence about the influence of RISC on lasing from a TADF emitter, namely, 2,3,5,6-tetrakis (carbazol-9-yl)-1,4-dicyanobenzene 4CzTPN doped in polystyrene (PS) microspheres (see in Figure 6). They claimed that the observed increase (decrease) in lasing intensity (SE lifetime) with temperature was caused by an accelerated depletion of singlet excitons promoted by the upconverted triplets. The use of TADF materials seems to be a promising approach to reduce the detrimental effect of triplets. Nevertheless, reports on the light amplification properties of such materials remain rare and further investigation on their photophysics is still needed.

4.2. Defined Star-Shaped Macromolecules

Dendrimers contain groups such as benzene,^[81] truxene,^[82] pyrene,^[83] or 1,4-diketo-2,3,5,6-tetraaryl-pyrrolo[3,4-c]pyrrole (DPP)^[84] and multiple functionalized arms. The absorption and luminescent properties can be tuned, for instance, by changing the nature of the core or length of the arms. Tsiminis et al. reported a study on the photophysics of dendrimers as a function of arm length. The dendrimers they studied contained benzene core and oligofluorene arms with different oligofluorene lengths.^[81] They observed absorption and emission spectra red shifts concomitant with PLQE increase from 40% to 55% as the arms were prolonged from 2 to 4 units. The ones with longer arms (3 and 4 fluorene units) exhibited lower DFB lasing thresholds (1.1 and 1.2 kW cm^{-2} for 3- and 4-fluorene unit arms, respectively) and higher slope efficiencies (5% and 6.6% for 3- and 4-fluorene unit arms, respectively). Truxene-cored dendrimers with three fluorene-based arms (named T1–T4 depending on the number of fluorene units) exhibited even better ASE/laser properties manifested by lower thresholds (0.515 kW cm^{-2} in T3), low loss coefficients (3.5 (T3) and 2.3 (T4) cm^{-1}), and high optical gain (38 (T3) and 20 (T4) cm^{-1}).^[82,85] Similarly, Xu et al. reported on an ASE study on a series of truxene-cored, pyrene-capped trigonal starburst conjugated molecules (TrPy, TrFPy, and TrF2Py) with zero, one, and two fluorene units in the arms and pyrene end-capping.^[86] Among these starburst molecules, TrF2Py showed the highest PLQE (60%) and better ASE performance at room temperature, whereas ASE’s performance in TrFPy was found to be more thermally stable (annealing up to 250° , the threshold increases only 4.5 times). The result suggested that the optimum oligofluorene arm length is a trade-off between ASE performance and thermal stability in these compounds.

Pyrene-cored dendrimers are also attractive fluorophores due to their high PLQE and carrier mobilities as well as excellent thermal stability.^[87] Uchimura et al. reported a series of pyrene-cored star-shaped molecules, 1,3,6,8-tetraarylpyrenes derivatives embedded in cholesteric liquid crystals (CLCs) for DFB lasing.^[88] Most of them showed a very high PLQE ($\approx 90\%$) and low lasing threshold. Xia et al. reported on the gain properties and laser stability of pyrene-cored 9,9-dihexylfluorene starbursts (P1–P3

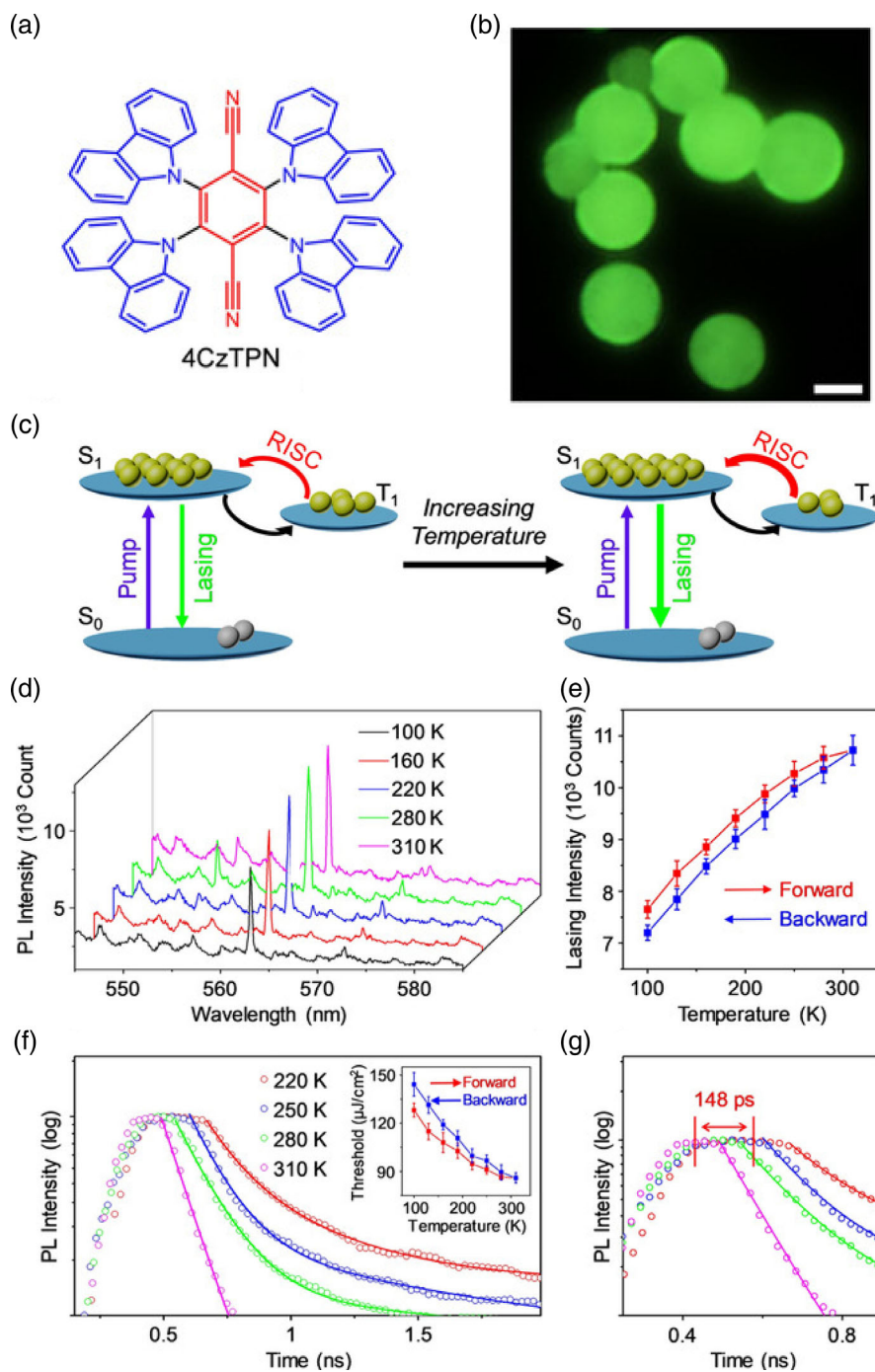


Figure 6. RISC-enhanced lasing action in TADF materials a) Chemical structure of 4CzTPN. b) PL image of 4CzTPN microspheres. c) Schematic illustration of the triplet-harvesting and boosting lasing process. d) Laser spectra of an isolated 4CzTPN-doped microsphere at different temperatures. e) Lasing intensity of the isolated microsphere as a function of temperature in forward and backward sweeps. f) Time-resolved PL (TRPL) decay curves of the lasing peak wavelength at different temperatures. Inset: Thresholds of an identical 4CzTPN-doped microsphere upon forward and backward sweeps as a function of temperatures. g) Magnification of the TRPL decay curves around the peak. In (d–g), the pump fluences were fixed at 1.7 times the value at the threshold. Reproduced with permission.^[34c] Copyright 2020, Wiley-VCH.

standing for 1–3 fluorene repeat units).^[83] These materials show a large optical gain coefficient (78 cm^{-1} for P2), high PLQE

(>95% for P2), low laser threshold ($0.15 \mu\text{J cm}^{-2}$), and large thermal stability (ASE unaffected up to 130°).

4.3. Polymers

4.3.1. Polyfluorenes

Poly(9,9-dioctylfluorene) (PFO) and its derivatives are a widely known polymeric gain medium family.^[19a,89] The photophysics and optical gain properties of polyfluorenes has been the subject of extensive investigation.^[20e,90] Xia et al. provided a comprehensive study on the gain properties of blue-emitting poly(9,9-dioctylfluorene-co-9,9-di(4-methoxy)phenylfluorene (F8DP), green-emitting F8BT, and red-emitting poly(fluorene-co-benzothiadiazole-co-thiophene-co-triphenylamine) (Red F). F8DP exhibited an ASE threshold ($E_{th, ASE}$) of 0.1 μJ and net gain coefficient (g) of 66 cm^{-1} and was found to outperform F8BT ($E_{th, ASE} = 0.45\text{ }\mu\text{J}$ and $g = 22\text{ cm}^{-1}$) and red-emitting Red F ($E_{th, ASE} = 0.45\text{ }\mu\text{J}$ and $g = 24\text{ cm}^{-1}$).^[89b] PFO is also known for its rich photophysics associated with a variety of conformational phases that the polymer adopts in a solid state, which can be triggered by applying different sample preparation protocols.^[91] Thus, amorphous randomly coiled phases coexist with metastable planar phases, aka β -phase, which attract attention due to their larger PLQE, vibronically resolved emission, improved carrier transport, and in general outperforming optical gain properties.^[92] Kuehne et al.^[93] reported the achievement of β -phase in a crosslinkable PFO derivative VE-PFO functionalized with vinyl ether side chains. Electron beam lithography could be applied to write DFB grating directly on the crosslinked polymer films, leading to lasing action from β -phase VE-PFO at a threshold as low as $0.4\text{ }\mu\text{J cm}^{-2}$ (grating period: 254 nm).

Side-chain engineering has shown to boost substantially both the optical and charge transport properties of PFO. Yap et al. reported two PFO-based copolymers containing 20% and 50% statistical fractions of short 9,9-di(2-methyl)butyl (F5) side-substituted fluorene units, namely, Y80F8:20F5 and S50F8:50F5.^[19a] Compared with PFO, the copolymers exhibited a much lower DFB laser threshold ($0.3\text{ }\mu\text{J cm}^{-2}$ for Y80F8:20F5 and $0.5\text{ }\mu\text{J cm}^{-2}$ for S50F8:50F5), enhanced PLQE (70% for Y80F8:20F5 and 60% for S50F8:50F5), and two orders of magnitude higher hole mobility ($3.7 \times 10^{-2}\text{ cm}^2\text{ V}^{-1}\text{ s}^{-1}$ for Y80F8:20F5 and $2.7 \times 10^{-2}\text{ cm}^2\text{ V}^{-1}\text{ s}^{-1}$ for S50F8:50F5). The basic electronic structure of polyfluorenes stayed unchanged while no additional luminescence quenching was introduced. The results were explained as due to the discrete number of F5 units behaving as bridge nodes for efficient exciton interchain hopping. A similar strategy of introducing a few short substituents among long substituents was also used to develop F8BT derivatives (XF1/4F8BT). XF1/4F8BT was obtained by inserting X% statistical content of branched 2-methylbutyl-substituted fluorene-co-benzothiadiazole units (F1/4) in the F8BT backbone chains.^[94] Although the optical gain properties of these copolymers were compromised by their limited solubility and modest film-forming property, their dispersion in F8BT or poly(9,9-dioctyl fluorene) (PFO) matrices led to a drop in ASE threshold from 17.45 to 11.02 and 0.94 kW cm^{-2} , respectively.

4.3.2. Phenylenevinylene Polymers (PPVs)

Poly(phenylenevinylenes) (PPVs) is another important family of conjugated polymers for light-emission applications. Tessler et al.

first demonstrated laser emission from PPVs using a high- Q microcavity structure for light oscillation in 1996.^[6b] Since then, different PPV derivatives were developed for light amplification covering large part of the visible spectral range. Poly[2,5-bis(2',5'-bis(2"-ethylhexyloxy)phenyl)-*p*-phenylene vinylene] (BBEHP-PPV) is a green-emitting polymer, which exhibits an ASE threshold of $1.1\text{ }\mu\text{J cm}^{-2}$ and PLQE of 86% in neat films. Incorporating it in 1,4-cyclohexanedimethanol divinyl ether (CHDV) polymerizable matrix leads to BBEHP-PPV/CHDV composites. BBEHP-PPV/CHDV can be casted on a periodically corrugated surface, such as on top of a blank DVD, and subsequently peeled off to yield a free-standing BBEHP-PPV/CHDV green laser with a threshold of 1.1 mJ cm^{-2} .^[95] Laser action in BBEHP-PPV DFB was also exploited as a highly sensitive fluorescent chemosensor. High sensitivity can be achieved with DFBs, thanks to their design, which allows direct contact between the gain layer and the analytes and the giant change of emission output caused by analyte quenchers when operated just above the lasing threshold.^[96] Namdas et al. reported another green-yellow lasing from poly 2,5-bis(3-tetradecylthiophen-2-yl) thieno[3,2-*b*] thiophene-C14 (also known as Super Yellow, SY) deposited in a LEFET architecture with nanoimprinted 1D and 2D DFB grating structures on top.^[97] Optically pumped lasing from SY was observed under no applied fields at a threshold as low as $3.6\text{ }\mu\text{J cm}^{-2}$. MEH-PPV is a highly efficient red-emitting gain medium which has been widely studied.^[98] Samuel and coworkers developed 2D DFB lasers with MEH-PPV on first- ($\Lambda = 268\text{ nm}$) and second- ($\Lambda = 409\text{ nm}$)-order gratings. In first-order DFB gratings, lasing from MEH-PPV occurred, peaking at 632 nm with an full width half maximum (FWHM) value of 0.74 nm and a threshold of 0.66 nJ.^[99] The use of second-order DFBs led to a lasing threshold increase to 4 nJ with a relatively higher slope efficiency of 6.8% and good output beam quality factor M^2 of 2.2.^[100] Martini et al. encapsulated MEH-PPV in the aligned nanopores of a silica host, leading to controlling the chain conformation to manipulate polarized, low-threshold ASE emission.^[101] Novel copolymers composed of two PPV derivatives, namely, poly((2-(20,50-bis(200-ethylhexyloxy)phenyl)-1,4-phenylenevinylene)-co-(2-methoxy-5-(20-ethylhexyloxy)-1,4-phenylenevinylene)) (BEHP-co-MEH-PPV), also demonstrated light amplification both in solution and in the solid state.^[102] BEHP-co-MEH-PPV membranes incorporated in quasiperiodic photonic crystal microcavities exhibited lasing at 607 nm with a threshold of $9\text{ }\mu\text{J cm}^{-2}$.

4.3.3. Ladder-Type Polymers

Ladder-type poly(*p*-phenylene) (LPPP) was first synthesized by Scherf and coworkers.^[103,104] It is a conjugated polymer composed of phenyl units connected at parapositions. Among LPPP, methyl-LPPP (MeLPPP) bearing methyl, *n*-hexyl, and 1,4-decyl-phenyl substituent groups on the backbone is probably the most characterized one.^[105] MeLPPP has been applied as active gain medium on poly(ethylene terephthalate) (PET) substrate during the early exploration of flexible DFB lasers.^[106] Compared with PFO, the SE band of MeLPPP is more extended due to less spectral overlap with the mid-visible photoinduced absorption band ascribed to polarons. It has very low intrachain disorder, leading

to narrow vibronically resolved emission which renders some possible new applications. For instance, nonequilibrium Bose–Einstein condensation of exciton–polaritons in microcavities was demonstrated in this polymer at room temperature.^[105] Laqui et al. investigated the photophysics of a series of ladder-type polymers, with different numbers (N) of bridged phenyl rings in the monomer, namely, poly(indenofluorene) (P2), poly(ladder-type tetraphenylene) (P3), poly(ladder-type pentaphenylene) (P4), and methyl-substituted ladder-type poly(phenylene) (MeLPPP). The spectral shift of the fluorescence spectrum found on polymers with different bridged phenyl ring numbers was described by a Kuhn fit instead of a simple $1/N$ dependence. Triplet absorption red shifted with the increasing number of phenyl rings and was constant until N reached 4. The ASE threshold also increased along with monomer length.^[107] ASE and optical gain characterization of these polymers were investigated and compared with the optical gain properties of carbazole containing poly(ladder-type tetraphenylene) (C1) and poly(ladder-type pentaphenylene) (C2).^[108] The carbazole-containing polymers showed a lower PLQE, less efficient gain, and higher ASE thresholds due to the more pronounced overlap of SE with the photoinduced absorption (PA) band. Kim et al. reported further development on novel alternating indenofluorene–phenanthrene copolymers named BLUE-1 and BLUE-2.^[109] In particular, BLUE-1 possessed outstanding optical gain coefficients as high as 154 cm^{-1} and a high hole mobility of $0.5\text{ cm}^2\text{ V}^{-1}\text{ s}^{-1}$ in the OFET device structure and $10^{-2}\text{ cm}^2\text{ V}^{-1}\text{ s}^{-1}$ measured with time of flight.

Chang et al. developed a novel set of ladder-type poly(indenofluorene) copolymers (namely, nLF-BT [$n = 2\text{--}4$], n depending on the length of the indenofluorene chain) for optical amplification. These copolymers incorporated indenofluorene chains with various lengths and 2,1,3-benzothiadiazole (BT) units possessing similar emission range but largely enhanced optical net gain compared with F8BT. Importantly, the copolymers exhibited ASE threshold unchanged upon annealing at temperatures as high as 160° .

4.4. Host–Guest Blends Coupled by Förster Resonant Energy Transfer

Förster resonant energy transfer (FRET) in host:guest blends of organic molecules or polymers is a very attractive mechanism to be exploited for optical gain. FRET is not really a novel concept for construction of highly efficient optical gain media. The idea^[6c,d,110] has already been demonstrated in the early days of organic lasers. Many merits of such design have been noted: first, under optimum resonant overlap conditions, low guest contents are required to achieve complete host-to-guest energy transfer. This is an advantage as large guest dilution has positive implications in the guest emission properties. Second, unlike passive matrices, conjugated host matrices provide large absorption of optical excitation, which also contributes in operating the lasers at low optical pump thresholds. Third, the emission is largely displaced from absorption, thus reducing self-absorption losses. Finally, it offers assets in terms of emission tunability. P3HT is commonly disregarded for light-emission polymers due its polycrystallinity and tendency for low emission. However, based on the concept of FRET, efficient ASE/lasing was demonstrated

from regioregular poly(3-hexylthiophene) P3HT when blended in a F8BT host.^[111] In a study of the FRET-assisted ASE behavior of the blends with different P3HT contents, it was found that almost 80% of the total harvested excitons in F8BT contributed to P3HT ASE, the other 20% being lost due to parallel deactivation pathways such as exciton–exciton annihilation.^[112] F8BT matrix dispersion enabled optical gain from another common p-type OPV material, poly[N-9'-heptadecanyl-2,7-carbazole-*alt*-5,5-(4',7'-di-2-thienyl-2',1',3'-benzothiadiazole)] (PCDTBT). It is noteworthy that PCDTBT pristine films did not exhibit SE in contrast with F8BT:PCDTBT blends, confirming that F8BT played a twofold role, reducing PCDTBT chain aggregation and acting as a host energy-transfer matrix. F8BT:PCDTBT blends exhibited red-to-near-infrared ASE and laser emission.^[113]

However, the match up of host and guest is not always straightforward as polymer blend demixing is often a problem.^[114] Due to the intrinsic dependence of FRET rate on host–guest average distances, the formation of enriched phases will reduce the energy-transfer efficiency. Another significant effect that is often detrimental for SE is the severe spectral overlap between guest SE and the host absorption bands arising from polarons or triplets. This effect is for instance visible in blends of PFO and F8BT. The PL of PFO is quenched upon mixing it with a 10–20 wt% of F8BT.^[114a] The resulting blends show green F8BT luminescence with PLQE values approaching 70%.^[114a,115] Despite the fact that both PFO and F8BT show optical gain properties when processed in pristine films,^[89b] no SE from F8BT is observed in the blends. This phenomenon is caused by polaron photogeneration in picosecond timescales in PFO and the spectral location of their absorption overlapping with F8BT SE. Indeed, the substitution of PFO by other energy-transfer matrices with reduced polaron yield has shown to reconstitute F8BT SE in the resulting blends.^[14b,40] When dispersing F8BT in a short conjugated fluorene-based host, namely, 3,6-*bis*(2,7-di([1,1'-biphenyl]-4-yl)-9-phenyl-9H-fluoren-9-yl)-9-octyl-9H-carbazole (DBPhFCz), larger exciton confinement is manifested in a much slower polaron formation rate, enabling the observation of ASE and lasing in DBPhFCz:F8BT blends with the lowest thresholds of 2.8 and $9.79\text{ }\mu\text{J cm}^{-2}$, respectively (see in **Figure 7**).^[40] In addition, DBPhFCz:F8BT blends exhibit outstanding thermal stability favored by the large glass transition temperature (308°) of DBPhFCz.^[40]

In a follow-up work, a range of homologous hosts with different fluorinated substituents, 9-octyl-3,6-*bis*(2,7,9-triphenyl-9H-fluoren-9-yl)-9H-carbazole (DPHS), 3,6-*bis*(2,7-*bis*(3,5-difluorophenyl)-9-phenyl-9H-fluoren-9-yl)-9-octyl-9H-carbazole (DF), and 3,6-*bis*(2,7-*bis*(3,5-*bis*(trifluoromethyl)phenyl)-9-phenyl-9H-fluoren-9-yl)-9-octyl-9H-carbazole (DCF3), were blended with F8BT showing notable ASE and lasing properties.^[14b] Host fluorination pushes down the highest (lowest) occupied molecular orbitals without significantly changing the energy gap between the highest occupied and lowest unoccupied molecular orbitals (HOMO and LUMO), the energy-transfer efficiency, nor the ASE thresholds of the host:F8BT blends. In this way, current injection and optical gain are separately tuned in the host and guest components, simplifying the design and synthesis of novel gain materials for electrically pumped lasers. Combining the enhancement in optical gain and thermal stability, with the limited diffusion of polaron pairs, the triplet scavenging properties shown by some

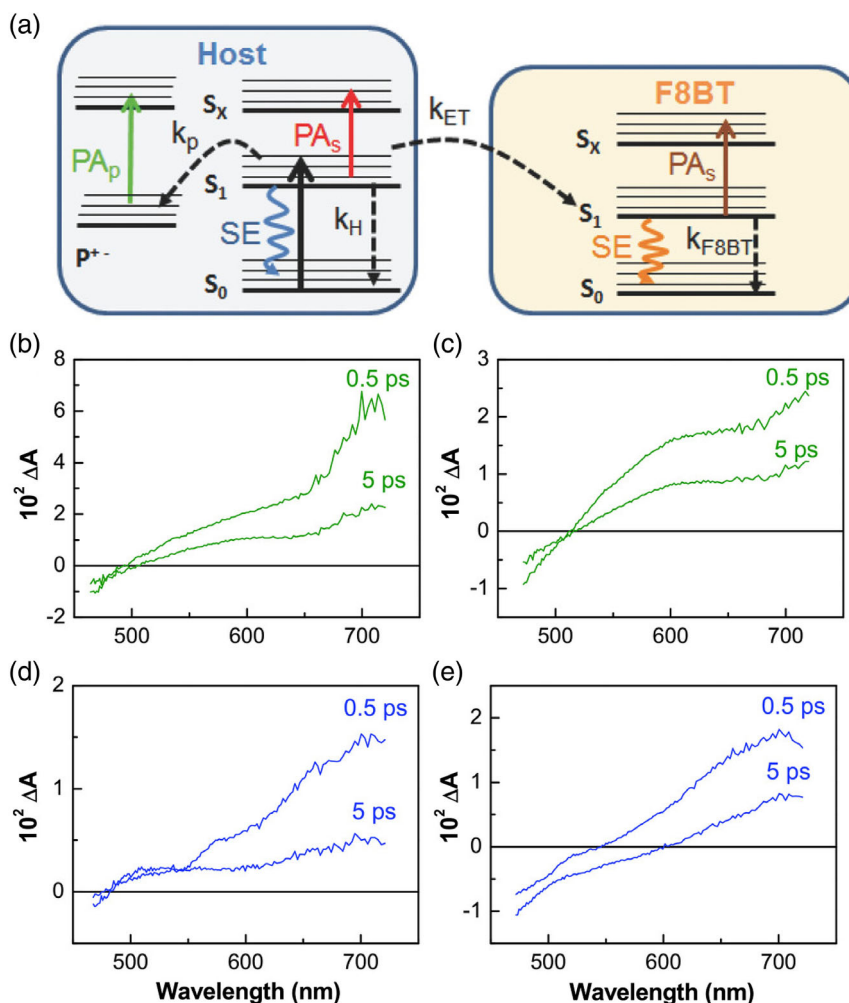


Figure 7. Example of gain medium using FRET energy-transfer system. a) Scheme of energy levels of blue-emitting host (left) and F8BT guest (right). b–e) Transient absorption (TA) spectra of the blend film using different hosts: PFO (green) and DBPhFcZ (blue). b) 1 wt% and c) 20 wt% F8BT with PFO and d) 1 wt% and e) 20 wt% F8BT with DBPhFcZ. About 0.5 and 5 ps in the TA spectra are the pump–probe delays following excitation at 387 nm with 150 fs, 200 nJ pulse⁻¹ (165 μJ cm⁻²). In PFO blend, no positive TA is observed in F8BT emission range (500–610 nm), indicating that PFO-based PAp overwhelms FRET-pumped F8BT SE. In the 1 wt% F8BT with DBPhFcZ blend, the TA spectra is similar to PFO blend (b) and (c). In the 20 wt% F8BT with DBPhFcZ blend, positive TA is observed in the 5 ps delay spectra showing that F8BT SE overcomes DBPhFcZ PAp. Reproduced with permission.^[40] Copyright 2018, Wiley-VCH.

hosts, and the simplification in materials design, e.g., energy-level match up, we believe that active host–guest blend systems based on FRET can play a very important role in the development of future electrically pumped organic lasers.

5. Typical Resonator Architectures

The resonator cavity provides optical feedback for light amplification. The resonator geometry defines the resonant modes supported by the cavity and the spatial characteristics of the output beam. Therefore, resonator design and implementation is crucial for the development of organic lasers of a high quality factor and low lasing thresholds. Resonators have different forms and shapes, which span from simple Fabry–Perot cavities to more complex geometries (see in **Figure 8** for some typical resonator geometries).

5.1. Microcavities

The simplest arrangement for an organic laser cavity is probably a Fabry–Pérot microcavity obtained by placing the organic gain medium between two highly reflective mirrors. The mirrors can be metallic or dielectric multilayers known as distributed Bragg reflectors (DBRs). The optical thickness of the microcavity is usually from a few hundred nanometers to a few microns. It is normally designed to match integer multiples of half-wavelength values.

The use of wedge-shaped cavities with varying cavity thicknesses along the axis allows for easy manipulation of the output laser modes.^[47d] The light confinement can be further improved by introducing lateral structures into the cavity.^[116] The conventional organic gain media used in the cavities are mainly amorphous thin films. However, single crystals can benefit from the

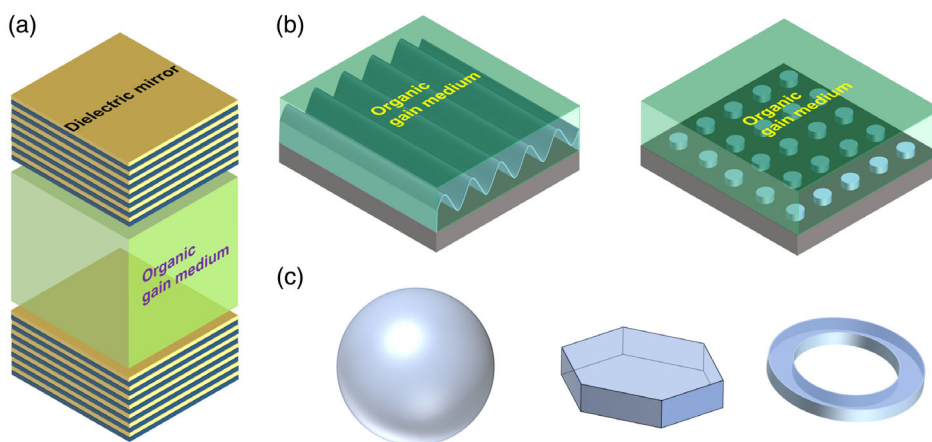


Figure 8. Resonator structures used for organic lasers. a) Planar DBR cavities. b) 1D and 2D DFB gratings. c) WGM cavities of different geometries, microspheres, microdiscs, and microrings (from left to right).

alignment of the dipole moment in the gain layer. An example is the work done by Yamashita et al. They developed DBR microcavities with thermally evaporated thiophene/phenylene co-oligomer (TPCO) single crystals as gain media. The resultant device achieved lasing at a threshold of 3 mJ cm^{-2} .^[117] Metallic oxides such as ZnO or SiO₂ are common choices as dielectric layers for DBR mirrors, although sometimes polymer DBR mirrors have also been used.^[118] Canazza et al. demonstrated lasers from F8BT with a surprisingly low threshold value ($<20 \mu\text{J cm}^{-2}$) in all-polymer DBR cavities fabricated by spin coating polyvinylcarbazole and cellulose acetate processed from orthogonal solvents.^[119]

Similar microcavity structures have also been implemented in OLEDs to achieve high color purity. As the OLED-based display industry becomes more mature, organic LDs could have an important market niche in the future, given that laser-based projection displays may have a prominent role in the next generation of display technologies. Compared with OLEDs, organic LDs would provide high color purity, coherence, and brightness resulting from laser features. There have been efforts to design and integrate microcavities with high *Q*-factors inside OLEDs to optimize their electrical/optical properties.^[120] Liu and coworkers reported work in this regard.^[121] To explain the spectral-narrowing phenomena in the DBR cavity-based LEDs, Wang et al. proposed that the optical field in the cavity induced resonant spatially extended states with characteristics similar to polarons. In the cavity-free LEDs based on F8BT (65 nm film thickness), no PL/EL signal could be observed under both photoexcitation and current injection. However, in the cavity-based LEDs, the presence of an optical field can extend the wavefunctions of Frenkel excitons, forming resonant spatially extended states with cooperative character. These aligned polaron-like states would relax into light-emitting states essentially, leading to spectrally narrowed PL/EL with linear polarization.^[122] Lin et al. reported narrow-band pure-UV (FWHM $\approx 9.95 \text{ nm}$) and blue (FWHM $\approx 8 \text{ nm}$) electroluminescence from microcavity OLEDs using 1,2-di-*p*-tolyl-1H-phenanthro[9,10-*d*]-imidazole (Tol-PPI) and BSB-Cz as emitters, respectively.^[123]

5.2. Diffractive Resonators

Diffractive resonators contain no mirrors but periodic nanostructures to diffract or scatter the light. This configuration exploits a periodic corrugation on the organic film surface for reflecting the propagating modes back and forth along the organic layer. Outcoming photons scattered by the periodic corrugations interfere constructively with incoming photons, leading to a standing “Bragg-scattered” wave in the direction along the waveguide. This mechanism depends on the photon wavelength (λ) and the corrugation period (Λ) and must fulfil the Bragg condition, $m\lambda = 2n_{\text{eff}}\Lambda$. Here, m is the order of the diffraction and n_{eff} is the effective refractive index of the waveguide. The full description of the mechanism has been discussed in detail by Kogelnik and Shank.^[124] Different diffractive structures are used for constructing diffractive resonators, e.g., 1D gratings, 2D/3D photonic crystal structures, and concentric circular gratings.

5.2.1. DFB Lasers with 1D Gratings

In general, optically pumped DFB organic lasers can achieve low threshold lasing due to the small mode volumes of DFB structures. This feature offers the prospect of optical pumping with low-end pulsed sources such as LEDs. There have been several demonstrations of DFB organic lasers pumped with pulsed nitride-based LEDs (see examples in **Figure 9**), a configuration that is often referred to as “indirect electrically pumped lasing.”^[7,8,125] The latest development of this aspect is demonstrated by Tsiminis et al. using a commercial InGaN LED (Philips Luxeon Rebel royal blue) to pump a DFB laser fabricated by BBEHP-PPV deposited on top of a nanoimprinted UV resist layer and encapsulated with a CYTOP cladding.^[8b] A clear laser peak at 533 nm with a well-defined fan-shaped output beam was achieved at an optical pump threshold of 770 W cm^{-2} . DFB lasers operating with the second diffraction order are the most common choices due to their simpler implementation. The second-order DFB lasers provide better light outcoupling properties, whereas first-order DFB lasers lead to lower lasing thresholds. The use of mixed-order DFB gratings can combine the

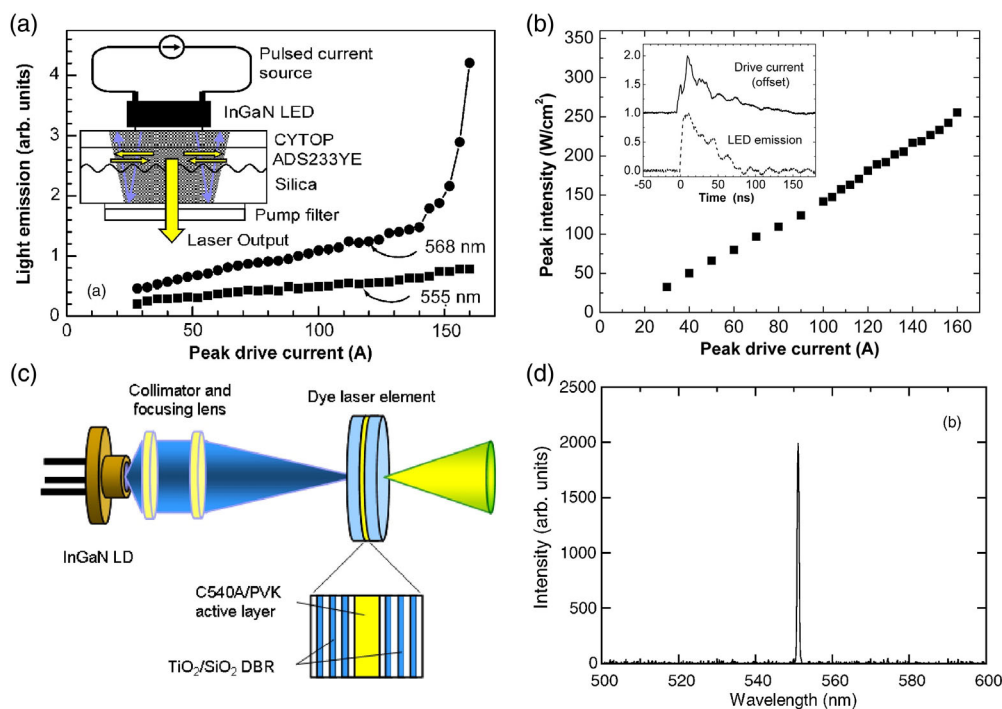


Figure 9. Indirectly electrically pumped organic laser. a) Output intensity from ADS223YE at 568 and 555 nm as a function of peak drive current. Inset: Schematic diagram of the InGaN LD-pumped polymer laser. b) Peak intensity of the light pulse of the Luxeon K2 LED as a function of drive current. Inset: A comparison of temporal characteristics of the drive current (top) and light output (bottom) of the LED. c) Schematic diagram of the diode-pumped polymeric dye (C540A-doped PVK, 1.2 μm) laser. Cavity is constructed with two DBRs (ten pairs of TiO₂/SiO₂ quarter-wave thin films). d) Lasing spectra at the pumping peak power of 24 mW. Reproduced with permission.^[8a] Copyright 2008, AIP, and^[125b] Copyright 2008, AIP.

advantages of the different orders of diffraction, producing lower thresholds and more efficient light extraction. A vast number of papers on organic DFB lasers were published in the past two decades. The most common DFB implementation method starts by developing a grating on a hard mold with e-beam lithography, often on a SiO₂-coated silicon wafer. This wafer serves as a substrate on which to deposit the organic layer. This method has however a limited throughput. It is costly and does not guarantee that the substrate can be reused many times. An alternative option is to use soft lithography techniques to transfer the nanostructures onto a soft mold based on an elastomer-based stamp onto a plastic substrate^[113,126] or directly on top of the organic gain layer.^[127]

Another advantage of DFB organic lasers is that the output wavelength can be tuned by changing the grating period and effective refractive index. This property has been used for the design of continuously tunable DFB lasers, exploiting fan-shaped grating geometries,^[128] or by mechanical period modification via bending or stretching^[129] of patterned plastic or elastomer-based substrates. Castro-Smirnov et al.^[126a] developed second-order DFB lasers based on periodically corrugated cellulose diacetate (CdA) with different periods ($\lambda = 278, 350, \text{ and } 416 \text{ nm}$). Conjugated polymer layers deposited on top of this DFB exhibited laser action in the blue, green, and red spectral region. They demonstrated that the lasing thresholds were scarcely affected by substrate bending despite undergoing a slight shift with the bending angle. In a recent report, Berdin et al. achieved a total tuning of 123 nm in the orange–red laser spectrum through

mechanical stretching of a periodically corrugated polyvinyl acetate (PVAc) substrate with embedded laser dyes.^[129b] The refractive index can be changed upon modification of the organic film thickness^[126a,130] or by changing the host/guest ratio if the film is based on host:guest blends of different organic compounds. In a recent report,^[40] Zhang et al. demonstrated a large laser emission tuning from 539 to 587 nm with the same DFB gratings by changing the ratio of the oligomer host and F8BT polymer guest and film thickness, also resulting in very low lasing thresholds.

5.2.2. 2D or 3D Photonic Crystals

2D photonic crystal structures enable 2D feedback in organic thin films, attracting great attention during the past two decades.^[131] They rely on a periodical 2D arrangement of features, typically holes on a substrate. Different geometries have been exploited including square, hexagonal, or concentric circular. Unlike 1D DFB structures, 2D DFB configurations provide optical feedback in different directions within the film plane, which offers more possibilities for controlling the spectral and spatial characteristics of laser output. Calzado et al.^[131c,132] fabricated 2D DFB grating structures directly on the active layers. More recently, Zhang et al.^[133] fabricated 1D and 2D DFB chirped cavities using modified interference lithography with UV laser beam. Due to the varied periods in the chirped cavities, continuous-emission spectral tuning was obtained by moving the pumping spot along the DFB.

Compared with 1D and 2D structures, the applications of 3D photonic crystals to organic lasers are less popular. Early reports on such structures are demonstrated by back-filling opals with polymers or dyes to observe ASE and lasing behavior.^[134] The use of 3D zirconia inverse opal photonic structures enabled lasing from liquid solutions of rhodamine dyes.^[135a] In a more recent report, 3D photonic crystals from self-assembled diamond-like structures were achieved in a polymer templating blue phase (BP) I.^[135b] The templated cells were filled with a 1 wt% concentration of pyrromethene 597, and a clear lasing peak at 565 nm emerged upon photoexcitation with a 681 nJ threshold energy.

5.2.3. Integration of DFB Structures into LEFET/OLED Devices

As mentioned earlier, metal electrodes can cause strong light absorption precluding optical gain. LEFET structures are attractive due to the carrier recombination and emission occurring in the area far away from the metallic electrodes. Gwinner et al. demonstrated optically pumped lasing in F8BT from a

rib-waveguide DFB structure consisting of tantalum pentoxide integrated within the channel of a top-gate/bottom-contact LEFET.^[45b] The optical pumping threshold was $4.5 \mu\text{J cm}^{-2}$ in the unbiased device which is comparable with the value measured without metal electrodes. This result suggested that the electrodes did not cause extra losses to the optical gain in this device configuration (see in **Figure 10**). Yamao et al. investigated the effect of current injection on ASE using a slab crystal of 2,5-bis[4-(5'-phenylthiophen-2'-yl)phenyl]thiophene (AC'7)-based LEFET. They demonstrated spectrally narrowed emission peaking at 556.3 nm with an FWHM of 2 nm under operating conditions. In this structure the diffraction gratings were placed on the gate insulator, i.e., silicon oxide, engraved with a focused ion beam. The control device without diffraction gratings showed a broad emission with an FWHM value of 42.1 nm.^[45c]

Different strategies have been proposed to minimize electrode losses in the OLED sandwich configuration. Examples include the use of ultrathick carrier transport layers, optical buffer layers, or aluminum-doped zinc oxide anodes. Song et al.^[45d] achieved tunable lasing from F8BT-based OLEDs equipped with nanoimprinted gratings on ZnO as charge injection layers. They

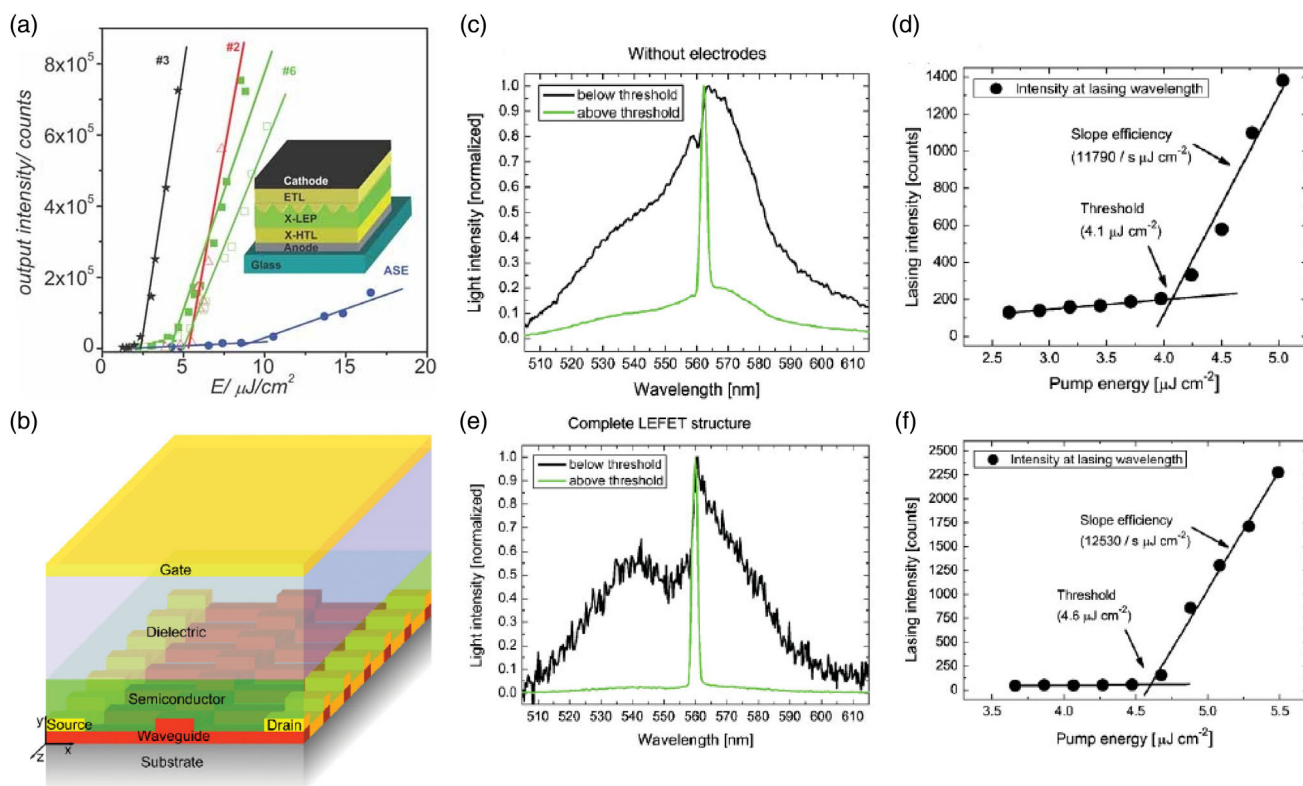


Figure 10. Exploration of optically pumped organic lasers in OLED and light emitting OFET device. a) Plot of the output versus excitation density (E) for device #2 (single emission layer of X-LEP, open triangle), device #3 (three-layer stack without electrodes: emission layer X-LEP sandwiched between 680 nm-thick X-HTL hole transport layer and 280 nm-thick ETL electron transport layer, stars), device #6 without applied field (fully functional OLED with optimized layer thicknesses, solid squares) and under electrical operation ($E = 7.9 \times 5 \text{ V cm}^{-1}$ and $j = 7 \text{ mA cm}^{-2}$, open squares), and ASE threshold of the electrically functional ASE device #7 (solid circles). The inset shows a schematic picture of device #6. b) Schematic illustration of an F8BT-based top-gate/bottom-contact LEFET structure with integrated waveguide rib and DFB grating. c) Emission spectra of the device in (b), without electrodes (325 nm PMMA), below and above the lasing threshold. d) Corresponding emission intensity versus pump energy at the lasing wavelength. e) Emission spectra of the device in (b), equipped with transistor electrodes and optimized gate architecture (430 nm PMMA, 10 nm Ag), below and above the lasing threshold. f) Corresponding emission intensity versus the pump energy at the lasing wavelength. Reproduced with permission.^[45a] Copyright 2010, Wiley-VCH, and^[45b] Copyright 2009, Wiley-VCH.

exploited the high refractive index of ZnO to confine waveguide modes far away from the electrodes, thus reducing optical losses. As a result, they observed higher PLQE values, lower ASE/lasing thresholds, and improved waveguiding properties with respect to control OLEDs without ZnO charge injection layers. Wallikewitz et al.^[45a] investigated the influence of electrical excitation on optical-pumped lasing from devices based on oxetane-functionalized poly(spirobifluorene) (X-LEP) as active layer (see in Figure 10). In this device, the DFB gratings were fabricated with holographic lithography on the photo-crosslinkable X-LEP. The presence of carrier transport layers in the device helped reduce the optical losses, therefore, enabling lasing. Yet, the presence of the metal electrodes on the other side of the carrier transport layers led to an increase in lasing threshold from $2.5 \mu\text{J cm}^{-2}$ (electrode-free configuration) to $4.8 \mu\text{J cm}^{-2}$. Importantly, they confirmed laser action even when a current density of 7 mA cm^{-2} was swept across the device, although the threshold further increased to $5.6 \mu\text{J cm}^{-2}$.

More recently, Sandanayaka et al.^[10] reported lasing from BSB-Cz in an inverted OLED device configuration with mixed one and two orders of DFB gratings ($\Lambda = 140$ and 280 nm), as shown in Figure 11. The gratings were engraved on SiO₂-coated indium tin oxide (ITO) using electron beam lithography and reactive ion etching. The complete geometry was ITO (100 nm)/20 wt% Cs:BSB-Cz (60 nm)/BSB-Cz (150 nm)/MoO₃ (10 nm)/Ag (10 nm)/Al (90 nm). The authors demonstrated the emergence of a narrow laser peak at 480 nm (FWHM < 0.2 nm), under current pulses of 600 A cm^{-2} density, 400 ns duration, and 1 kHz repetition rate. This important milestone is probably the first clear evidence of electrically

pumped lasing in an organic semiconductor. Although the required current densities to achieve lasing are yet impractical in terms of applications, the results are promising and pave the way for future developments in the field. Noteworthy, Ahmad et al. recently reported on a comprehensive electrical model to obtain the transient populations of electrons, holes, polarons, triplets, and singlet excitons as a function of time in an OLED under electrical pumping, assuming a real nonuniform spatial distribution of the electric field.^[136] They confirmed that the maximum singlet population (and thus the suitable timing for laser action) occurs within a narrow time window between the e-h recombination and triplet (polaron)/singlet annihilation time events. Importantly, the required current densities estimated to achieve lasing are well above those values obtained from optical measurements (singlet populations obtained from optical pumping threshold). This new methodology could be an interesting tool to pinpoint materials and device design to achieve lasing under current injection.

5.3. WGM Resonators

WGM resonators are based on the principle that light can be trapped in a high-refractive-index medium with an annular or spheric shape to form a closed loop. The light is guided in the loop by multiple total internal reflections on the curved resonator/ambient interface and eventually returns to its origin. If photons meet in phase, the process can lead to constructive interference and formation of an optical mode. In the case that the propagation wavelengths overlap well with the emission spectrum of the gain medium, the light will be amplified.

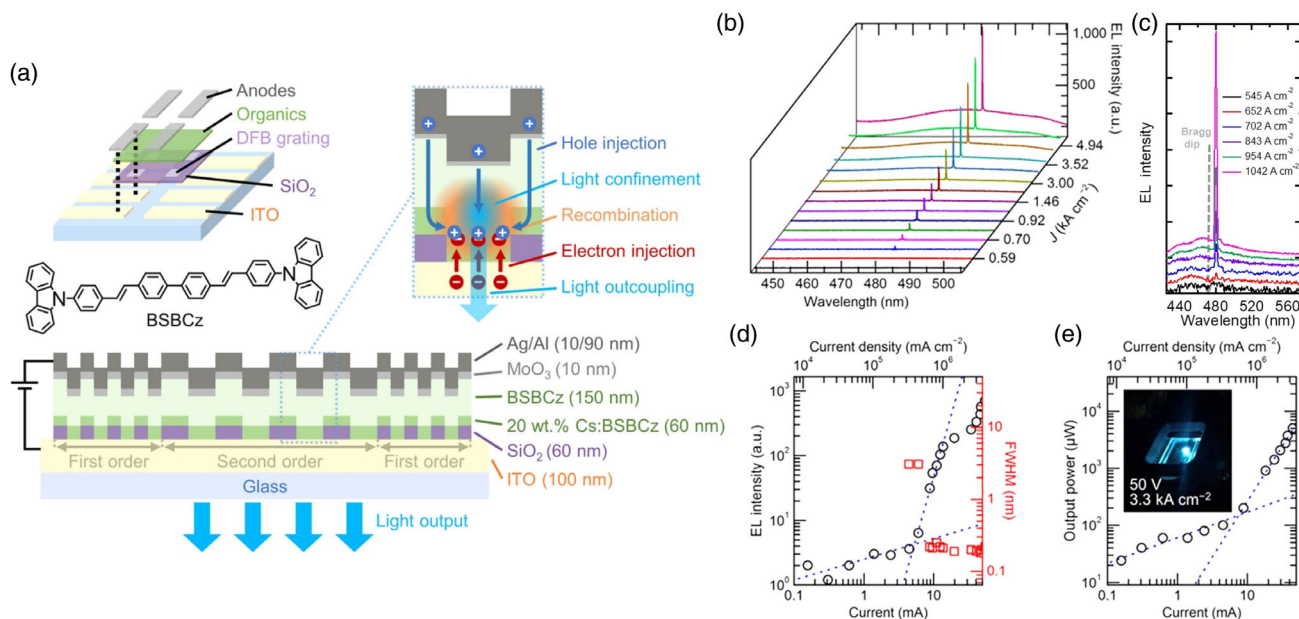


Figure 11. Lasing action under current injection in an OLED device with DFB gratings. a) Schematic representation of the structure used for electrically pumped organic laser (SiO₂ widths of 140 and 70 nm for second- and first-order gratings, respectively). b) Emission spectra at different injected current densities collected in the direction normal to the substrate in the device. c) PL spectra around the lasing threshold (the dashed line indicates the Bragg dip). d) Output intensity and FWHM versus the driving current. e) Output power versus the driving current. The inset shows a photograph of a device under pulse operation at 50 V. The laser emission is collected with an optical fiber connected to a multichannel spectrometer, PMA50. Reproduced with permission.^[10] Copyright 2019, IOPscience.

Such resonators always show extremely low losses, very-high-quality factors, and narrow bandwidths. An interesting feature is that these structures can be easily implemented from solution process methods. Therefore, organic semiconductors are highly suitable for WGM lasers. For example, one can easily fabricate a microring with polymers by dipping a silica fiber into concentrated solution. The outside surface of the fiber will be covered by a thin film of polymer upon dipping the fiber into the polymer solution. WGM resonators can be realized as microspheres, microdisks, microrings, microgoblets, or microcones on organic semiconductors with various methods.

One advantage of WGM resonators is that the Q -factor can be very high. Grudin et al.^[137] reported the highest optical quality factor of 6.3×10^{10} in a CaF₂ cavity. High Q -factor and low-loss features of such WGM microcavities enable very low lasing thresholds, which are in principle affordable under the so-called diode-pumped regime. WGM lasers have been developed, for instance, from conical PMMA microcavities coated with Alq₃: 4-(dicyanomethylene)-2-methyl-6-(4-dimethylaminostyryl)-4H-pyran (DCM). Lasing at 653 nm was achieved upon pumping with a low-cost conventional Blu-ray burner LD, which provided power source delivering 20 ns pulses at 500 Hz repetition rates.^[138] Laser performance has been compared between Fabry–Pérot microcavities based on 1D microwires (1D-MWs) and WGM microcavities from 2D rhombic microdisks (2D-RMDs) made of *p*-distyrylbenzene (DSB) microcrystals. The results showed a twofold reduction in lasing threshold in 2D-RMDs.^[139] It must be noted that a smooth defect-free surface is critical to enhance the optical quality of the resonators. Some scientists made use of extremely smooth air–liquid interfaces to achieve multicolored WGM lasers from droplets containing dyes (rhodamine 560 [R560] and rhodamine 640 [R640] in benzyl alcohol).^[140] Connected to this concept, CLC microdroplets have also been used for the same purpose.^[141] Laser tuning was achieved by changing the size of the droplets or temperature due to the temperature dependence of the refractive index of the CLCs.

WGM resonators have wide application prospects due to their low threshold, high sensitivity, and compactness.^[142–145] Such resonators can be used as luminescent chemosensors, offering very high sensitivity due to their high Q -factor and smaller bandwidths.^[142] Francois et al. tracked the real-time adsorption kinetics of bovine serum albumin using WGM laser action from Nile red-doped polystyrene beads.^[143] When photoexcited just above the threshold, an eight-times-high signal-to-noise ratio was achieved.

5.4. Random Lasers

Unlike the cavity geometries discussed above, in some cases, lasing action can also be achieved in the absence of geometrically defined resonator structures. In these circumstances, light travelling within the medium experiences multiple scattering and interference which can supply positive feedback. Distributed scattering centers, such as impurities, defects, and morphology variations, lead to the formation of instable cavities and closed loops of light path. Until now, the random lasing action has been observed in various disorder systems: nanoparticle-doped dye

solutions, liquid crystals, nanofibers, or polymer films. Random lasing resulting from substantial scattering was observed in spin-coated films of 2,5-dioctyloxy poly(*p*-phenylenevinylene) (DOO-PPV).^[146] Bai et al. also found random lasing in the planar waveguides of two novel steric hindrance-functionalized derivatives of F8BT, i.e., poly(9,9-diarylfuorene-altbenzothiadiazole) (FDFBT) and poly(9,9-diarylfuorene-4-carbazole-altbenzothiadiazole) (FCzBT).^[147] Upon inducing wrinkles or corrugation on the substrate, Anni et al.^[148] studied the correlations between random lasing behavior and the parameters of scattering centers in the PFO thin films. They concluded that light amplification in waveguides can be translated into random lasing only with suitable scattering conditions. Sarkar et al. demonstrated an effective approach to reduce the random lasing threshold of DCM-doped poly(vinyl alcohol) (PVA) film sandwiched between the opal structure, in which the photonic stop band overlaps with the emission range.^[149]

Due to the lack of a well-defined resonator geometry, emission tuning becomes a problem for early-stage random lasers. One possible solution is to take advantage of the mechanically flexible feature of organic films on top of soft substrates. Lee et al. fabricated tunable random lasers with Rhodamine 6G (R6G) and silver nanoprisms on polyethylene terephthalate (PET) substrates based on the resonance coupling between the photons and localized surface plasmon.^[150] In a recent report,^[151] Li et al. prepared a substrate with micropapilla surface structures from the natural lotus leaf via soft lithography. Well-recognized random lasing peaks were achieved using 4-(Dicyanomethylene)-2-tert-butyl-6(1,1,7,7-tetramethyljulolidyl-9-enyl)-4H-pyran (DCJTB) as gain medium. They observed the emission wavelength tuning by moving the pumping area or bending the substrate, which enabled for a 15 nm spectral tuning. This concept can be further developed for monitoring the instantaneous physiological phenomenon in biological imaging with lower noise.^[152] In polymer fibers, incorporating porous structures can produce a so-called inverted photonic glass, which leads to tunable random lasing by simply bending the fiber.^[153] Metal–organic framework (MOF) nanostructures have also been used as scattering centers for random lasing. The spectra of random lasers were modulated by thermal control of intramolecular charge transfer states in the laser dyes.^[154]

Random lasers draw attention not only due to the fascinating photophysics of the disorder system but also its advantages of simple manufacturing technology compared with traditional DFB or DBR lasers. For instance, Hsu et al. introduced 3D printing technology in random laser filament fabrication using a commercially available PVA matrix, a stilbene 420 laser dye, and TiO₂ particles, offering opportunities for low-cost, easily accessible laser devices.^[155] Nevertheless, organic random lasers have the potential to be light sources for compact, portable, and low-cost applications such as sensing. Spin-coated hybrid films of poly(triphenylamine-alt-phenylene vinylene) (TPA-PPV) and PS containing well-dispersed TiO₂ nanoparticles exhibited clear random lasing peaks, which can be used as remote sensors for 2,4,6-trinitrotoluene (TNT) vapors. Random lasing from the fully biofriendly silk inverse opals (SIOs) comprising silk protein and fluorescein sodium was also applied as a sensor for vapors of hydrogen chloride.^[156]

5.5. Polariton Laser

A polariton is a coupled state of a photon and an excited state, such as an exciton. When a photon and an exciton locate inside a suitable optical feedback structure, such as a DBR cavity, strong coupling of excitons and photons leads to the appearance of a new eigenstate known as a polariton, which behaves as a bosonic quasiparticle. Polariton lasing can be achieved at much lower pump thresholds than conventional lasing because it can take place without population inversion.^[157] However, in inorganic semiconductors, polaritons are stable only at cryogenic temperatures due to the characteristic low binding energy of Mott–Wannier excitons. In contrast, in organic semiconductors, excitons are tightly bound as a result of the low dielectric constant of the medium and polaritons are stable even at room temperature. The very first report on strong exciton–photon coupling in an organic semiconductor dates from 20 years ago and was achieved in tetra-(2,6-*t*-butyl)phenol-porphyrin zinc by Lidzey and coworkers.^[158] The first room-temperature polariton laser was reported by Kéna-Cohen et al., using a 120 nm-thick melt-grown anthracene single crystal sandwiched between two DBR mirrors (12 pairs of alternative SiN_{1.94} and SiO₂ layers).^[157] The threshold of polariton lasing was well below that of photon lasing in similar conditions. Followed by the observation of analogous behavior in a thermal-evaporated small-molecule layer^[159] and a spin-coated polymer layer (MeLPPP),^[160] the concept was quickly expanded. In a more recent report,^[161] a highly disordered spin-coated PFO film (with a much wider excitonic linewidth) was used as the active layer, showing a polariton threshold as low as 27.7 μJ cm⁻² (one order of magnitude lower than the previous report in polymer polariton lasing). Rajendran et al. investigated low-threshold (17 μJ cm⁻²) polariton lasing from a spin-coated pentafluorene layer (105 nm thick).^[162] A 10 nm-thick LiF protective layer was used in fabrication for further top DBR mirrors deposition. Qu et al. investigated the temperature dependence (from 16 K to room temperature) of polariton lasing behavior in 2,7-bis[9,9-di(4-methylphenyl)-fluoren-2-yl]-9,9-di(4-methylphenyl)-fluorene microcavities.^[163] They found that at a low temperature (<45 K), inefficient phonon–polariton interactions led to change in polariton population and eventually increase in the polariton lasing threshold. Putintsev et al.^[164] demonstrate quasi-steady-state polariton lasing (nanosecond scale) in a BODIPY-Br dye λ/2 planar microcavity. Under 4 ns-long nonresonant excitation, 1.2 ns polariton lasing was achieved, being four orders of magnitude longer than the inherent polariton lifetime. These latest studies provide valuable insights into the fundamental physical mechanisms of nonequilibrium polariton condensation. In future, polariton lasers may open a path for the realization of electrically pumped organic lasers.

6. Outlook and Further Development in Organic Lasers

Although optically pumped organic lasers have been demonstrated for more than 20 years, the realization of electrically pumped organic semiconductor lasers is still not satisfactorily demonstrated. The further development of electrically pumped organic lasers in the near future is subject to the establishment

of more precise materials design rules to overcome the limitations in terms of the charge transport and absorption losses discussed in Section 3. As summarized in Sections 4, a myriad of organic semiconductor materials including small molecules, dendrimers and polymers have already been designed and synthesized in the past years, which have not only led to improved optoelectronic properties but also better understandings of the inherent physics of organic semiconductors. In fact, some groups have made claims of electrically pumped organic lasers.^[10,121] These claims lack broad recognition even inside the organic optoelectronics community, not to mention scientists who are not specialized in the field. Without the aim of questioning these results, we remark that the difficulty to find suitable materials and the complexity of the device structures required to achieve electrically pumped lasing could both be the reasons in explaining the cautious atmosphere since these claims were made.

The development of the organic diode laser requires also further engineering solutions to obstacles regarding current injection, e.g., electrode and cavity fabrication. Transformative innovation may be necessary for device configuration. Based on the irreplaceable features of organics such as mechanical flexibility, chemically tunability, and biocompatibility, compared with their inorganic competitors, organic laser will play a very important role in future applications in illumination, communication, sensing, etc. OLEDs can be regarded as the template for organic lasers, which has already dominated high-end display plane marketplace. Nevertheless, the present-day success of OLEDs is built on billions of inputs and tens of years of continuous research and development. From this point of view, the final success of organic laser is properly just around the next corner.

Acknowledgements

R.X. acknowledges funding from National Natural Science Foundation of China (grants 61874058, 51861145301, 61376023), the Synergetic Innovation Center for Organic Electronics and Information Displays, and the Priority Academic Program Development Fund of Jiangsu Higher Education Institutions (PAPD-YX030003) in China. J.C.-G. acknowledges support from the Regional Government of Madrid through NMAT2D-CM project (S2018/NMT-4511) and RTI2018-097508-B-I00 (AMAPOLA). IMDEA Nanociencia acknowledges support from the “Severo Ochoa” Programme for Centers of Excellence in R&D (MINECO, grant SEV-2016-0686).

Conflict of Interest

The authors declare no conflict of interest.

Keywords

continuous wave pumping, electrically pumping, laser resonators, organic laser diodes, organic semiconductors

Received: November 21, 2020

Revised: January 17, 2021

Published online: February 25, 2021

- [1] T. H. Maiman, *Nature* **1960**, *187*, 493.
- [2] B. H. Soffer, B. B. McFarlan, *Appl. Phys. Lett.* **1967**, *10*, 266.
- [3] N. Karl, *Phys. Status Solidi A* **1972**, *13*, 651.
- [4] a) C. W. Tang, S. A. Vanslyke, *Appl. Phys. Lett.* **1987**, *51*, 913; b) C. W. Tang, S. A. Vanslyke, C. H. Chen, *J. Appl. Phys.* **1989**, *65*, 3610; c) J. H. Burroughes, D. D. C. Bradley, A. R. Brown, R. N. Marks, K. Mackay, R. H. Friend, P. L. Burns, A. B. Holmes, *Nature* **1990**, *347*, 539.
- [5] D. Moses, *Appl. Phys. Lett.* **1992**, *60*, 3215.
- [6] a) F. Hide, M. A. DiazGarcia, B. J. Schwartz, M. R. Andersson, Q. B. Pei, A. J. Heeger, *Science* **1996**, *273*, 1833; b) N. Tessler, G. J. Denton, R. H. Friend, *Nature* **1996**, *382*, 695; c) M. Berggren, A. Dodabalapur, R. E. Slusher, Z. Bao, *Nature* **1997**, *389*, 466; d) V. G. Kozlov, V. Bulovic, P. E. Burrows, S. R. Forrest, *Nature* **1997**, *389*, 362; e) D. G. Lidzey, D. D. C. Bradley, M. S. Skolnick, T. Virgili, S. Walker, D. M. Whittaker, *Nature* **1998**, *395*, 53; f) T. Virgili, D. G. Lidzey, D. D. C. Bradley, G. Cerullo, S. Stagira, S. De Silvestri, *Appl. Phys. Lett.* **1999**, *74*, 2767.
- [7] a) T. Riedl, T. Rabe, H. H. Johannes, W. Kowalsky, J. Wang, T. Weimann, P. Hinze, B. Nehls, T. Farrell, U. Scherf, *Appl. Phys. Lett.* **2006**, *88*, 241116; b) S. Klinkhammer, X. Liu, K. Huska, Y. Shen, S. Vanderheiden, S. Valouch, C. Vannahme, S. Braese, T. Mappes, U. Lemmer, *Opt. Express* **2012**, *20*, 6357; c) C. Karnutsch, M. Stroisch, M. Punke, U. Lemmer, J. Wang, T. Weimann, *IEEE Photonics Technol. Lett.* **2007**, *19*, 741.
- [8] a) Y. Yang, G. A. Turnbull, I. D. W. Samuel, *Appl. Phys. Lett.* **2008**, *92*, 163306; b) G. Tsiminis, Y. Wang, A. L. Kanibolotsky, A. R. Inigo, P. J. Skabara, I. D. W. Samuel, G. A. Turnbull, *Adv. Mater.* **2013**, *25*, 2826.
- [9] F. Hide, P. Kozodoy, S. P. DenBaars, A. J. Heeger, *Appl. Phys. Lett.* **1997**, *70*, 2664.
- [10] A. S. D. Sandanayaka, T. Matsushima, F. Bencheikh, S. Terakawa, W. J. Potscavage, C. Qin, T. Fujihara, K. Goushi, J.-C. Ribierre, C. Adachi, *Appl. Phys. Express* **2019**, *12*, 061010.
- [11] a) I. D. W. Samuel, E. B. Namdas, G. A. Turnbull, *Nat. Photonics* **2009**, *3*, 546; b) Y. Tian, Z. Gan, Z. Zhou, D. W. Lynch, J. Shinar, J.-H. Kang, Q. H. Park, *Appl. Phys. Lett.* **2007**, *91*, 143504.
- [12] a) I. D. W. Samuel, G. A. Turnbull, *Chem. Rev.* **2007**, *107*, 1272; b) M. D. McGehee, A. J. Heeger, *Adv. Mater.* **2000**, *12*, 1655; c) A. J. C. Kuehne, M. C. Gather, *Chem. Rev.* **2016**, *116*, 12823; d) C. Grivas, M. Pollnau, *Laser Photonics Rev.* **2012**, *6*, 419; e) Y. Jiang, Y. Liu, X. Liu, H. Lin, K. Gao, W. Lai, W. Huang, *Chem. Soc. Rev.* **2020**, *49*, 5885; f) C. Adachi, A. S. D. Sandanayaka, *CCS Chem.* **2020**, *2*, 1203.
- [13] M. D. McGehee, M. A. Diaz-Garcia, F. Hide, R. Gupta, E. K. Miller, D. Moses, A. J. Heeger, *Appl. Phys. Lett.* **1998**, *72*, 1536.
- [14] a) Q. Zhang, Y. Wu, S. Lian, J. Gao, S. Zhang, G. Hai, C. Sun, X. Li, R. Xia, J. Cabanillas-Gonzalez, Y. Mo, *Adv. Opt. Mater.* **2020**, *8*, 2000187; b) Q. Zhang, Q. Wei, X. Guo, G. Hai, H. Sun, J. Li, R. Xia, Y. Qian, S. Casado, J. R. Castro-Smirnov, J. Cabanillas-Gonzalez, *Adv. Sci.* **2019**, *6*, 1801455.
- [15] a) M. Goossens, A. Ruseckas, G. A. Turnbull, I. D. W. Samuel, *Appl. Phys. Lett.* **2004**, *85*, 31; b) A. Charas, A. L. Mendonca, J. Clark, L. Bazzana, A. Nocivelli, G. Lanzani, J. Morgado, *J. Polym. Sci. Part B: Polym. Phys.* **2011**, *49*, 52.
- [16] J. Dhguru, W. Liu, W. G. Gonzalez, W. M. Babinchak, J. Miksovskva, R. Landgraf, J. N. Wilson, *J. Org. Chem.* **2014**, *79*, 4940.
- [17] a) E. Ishow, A. Brosseau, G. Clavier, K. Nakatani, P. Tauc, C. Fiorini-Debuisschert, S. Neveu, O. Sandre, A. Leaustic, *Chem. Mater.* **2008**, *20*, 6597; b) J. N. Zhang, H. Kang, N. Li, S. M. Zhou, H. M. Sun, S. W. Yin, N. Zhao, B. Z. Tang, *Chem. Sci.* **2017**, *8*, 577.
- [18] a) A. R. Johnson, S.-J. Lee, J. Klein, J. Kanicki, *Rev. Sci. Instrum.* **2007**, *78*, 096101; b) J. C. de Mello, H. F. Wittmann, R. H. Friend, *Adv. Mater.* **1997**, *9*, 230.
- [19] a) B. K. Yap, R. Xia, M. Campoy-Quiles, P. N. Stavrinou, D. D. C. Bradley, *Nat. Mater.* **2008**, *7*, 376; b) T. Virgili, D. Marinotto, C. Manzoni, G. Cerullo, G. Lanzani, *Phys. Rev. Lett.* **2005**, *94*, 4; c) T. Virgili, D. Marinotto, G. Lanzani, D. D. C. Bradley, *Appl. Phys. Lett.* **2005**, *86*, 091113.
- [20] a) M. Sim, J. Shin, C. Shim, M. Kim, S. B. Jo, J.-H. Kim, K. Cho, *J. Phys. Chem. C* **2014**, *118*, 760; b) O. V. Mikhnenko, M. Kuik, J. Lin, N. van der Kaap, T. Q. Nguyen, P. W. M. Blom, *Adv. Mater.* **2014**, *26*, 1912; c) R. X. Meng, Y. Li, C. Li, K. Gao, S. Yin, L. X. Wang, *Phys. Chem. Chem. Phys.* **2017**, *19*, 24971; d) L. Lueer, C. Manzoni, G. Cerullo, G. Lanzani, Z. V. Vardeny, *Chem. Phys. Lett.* **2007**, *444*, 61; e) M. Ariu, M. Sims, M. D. Rahn, J. Hill, A. M. Fox, D. G. Lidzey, M. Oda, J. Cabanillas-Gonzalez, D. D. C. Bradley, *Phys. Rev. B* **2003**, *67*, 195333.
- [21] R. H. Friend, D. D. C. Bradley, P. D. Townsend, *J. Phys. D: Appl. Phys.* **1987**, *20*, 1367.
- [22] A. P. Monkman, H. D. Burrows, L. J. Hartwell, L. E. Horsburgh, I. Hamblett, S. Navaratnam, *Phys. Rev. Lett.* **2001**, *86*, 1358.
- [23] J. A. Veerman, M. F. Garcia-Parajo, L. Kuipers, N. F. van Hulst, *Phys. Rev. Lett.* **1999**, *83*, 2155.
- [24] a) O. G. Peterson, J. P. Webb, W. C. McColgin, J. H. Eberly, *J. Appl. Phys.* **1971**, *42*, 1917; b) H. Ohkita, S. Cook, T. A. Ford, N. C. Greenham, J. R. Durrant, *J. Photochem. Photobiol. A* **2006**, *182*, 225; c) S. Schols, A. Kadashchuk, P. Heremans, A. Helffer, U. Scherf, *ChemPhysChem* **2009**, *10*, 1071; d) L. Paul, A. Banerjee, A. Paul, K. Ruud, S. Chakrabarti, *J. Phys. Chem. Lett.* **2018**, *9*, 4314; e) M. Lehnhardt, T. Riedl, T. Weimann, W. Kowalsky, *Phys. Rev. B* **2010**, *81*, 165206.
- [25] M. Lehnhardt, T. Riedl, T. Rabe, W. Kowalsky, *Org. Electron.* **2011**, *12*, 486.
- [26] a) M. A. Baldo, R. J. Holmes, S. R. Forrest, *Phys. Rev. B* **2002**, *66*, 035321; b) T. Rabe, P. Görrn, M. Lehnhardt, M. Tilgner, T. Riedl, W. Kowalsky, *Phys. Rev. Lett.* **2009**, *102*, 137401; c) D. W. McBranch, B. Kraabel, S. Xu, R. S. Kohlman, V. I. Klimov, D. D. C. Bradley, B. R. Hsieh, M. Rubner, *Synth. Met.* **1999**, *101*, 291; d) E. J. W. List, C. H. Kim, A. K. Naik, U. Scherf, G. Leising, W. Graupner, J. Shinar, *Phys. Rev. B* **2001**, *64*, 155204; e) R. Osterbacka, M. Wohlgenannt, M. Shkunov, D. Chinn, Z. V. Vardeny, *J. Chem. Phys.* **2003**, *118*, 8905.
- [27] O. J. Korovyanko, R. Österbacka, X. M. Jiang, Z. V. Vardeny, R. A. J. Janssen, *Phys. Rev. B* **2001**, *64*, 235122.
- [28] W. Holzer, A. Penzkofer, T. Tsuboi, *Chem. Phys.* **2005**, *308*, 93.
- [29] a) C.-L. Lee, X. Yang, N. C. Greenham, *Phys. Rev. B* **2007**, *76*, 245201; b) N. J. Cheetham, M. Ortiz, A. Perevedentsev, L.-I. Dion-Bertrand, G. M. Greetham, I. V. Sazanovich, M. Towrie, A. W. Parker, J. Nelson, C. Silva, D. D. C. Bradley, S. C. Hayes, P. N. Stavrinou, *Chem. Mater.* **2019**, *31*, 6787.
- [30] a) J. Cabanillas-Gonzalez, M. R. Antognazza, T. Virgili, G. Lanzani, C. Gadermaier, M. Sonntag, P. Stroehriegel, *Phys. Rev. B* **2005**, *71*, 155207; b) T. Virgili, J. Clark, J. Cabanillas-Gonzalez, L. Bazzana, K. C. Vishnubhatla, R. Osellame, R. Ramponi, G. Lanzani, *J. Mater. Chem.* **2010**, *20*, 519.
- [31] M. Lehnhardt, T. Riedl, U. Scherf, T. Rabe, W. Kowalsky, *Org. Electron.* **2011**, *12*, 1346.
- [32] S. Schols, L. V. Willigenburg, S. Steudel, J. Genoe, P. Heremans, *IEEE J. Quantum Electron.* **2010**, *46*, 62.
- [33] a) A. S. D. Sandanayaka, T. Matsushima, F. Bencheikh, K. Yoshida, M. Inoue, T. Fujihara, K. Goushi, J.-C. Ribierre, C. Adachi, *Sci. Adv.* **2017**, *3*, e1602570; b) B. S. B. Karunathilaka, U. Balijapalli, C. A. M. Senevirathne, Y. Esaki, K. Goushi, T. Matsushima, A. S. D. Sandanayaka, C. Adachi, *Adv. Funct. Mater.* **2020**, *20*, 2001078; c) V. T. N. Mai, A. Shukla, A. M. C. Senevirathne, I. Allison, H. Lim, R. J. Lepage, S. K. M. McGregor, M. Wood,

- T. Matsushima, E. G. Moore, E. H. Krenke, A. S. D. Sandanayaka, C. Adachi, E. B. Namdas, S.-C. Lo, *Adv. Opt. Mater.* **2020**, *8*, 2001234.
- [34] a) H. Nakanotani, T. Furukawa, C. Adachi, *Adv. Opt. Mater.* **2015**, *3*, 1381; b) H. Nakanotani, T. Furukawa, T. Hosokai, T. Hatakeyama, C. Adachi, *Adv. Opt. Mater.* **2017**, *5*, 1700051; c) Y. S. Zhao, Z. Zhou, C. Qiao, K. Wang, J. Liang, Z. Wei, H. Dong, C. Zhang, Y. Yan, L. Wang, Q. Peng, Z. Shuai, *Angew. Chem., Int. Ed.* **2020**, *59*, 21677; d) H. Ye, D. H. Kim, X. Chen, A. S. D. Sandanayaka, J. U. Kim, E. Zaborova, G. Canard, Y. Tsuchiya, E. Y. Choi, J. W. Wu, F. Fages, J.-L. Bredas, A. D'Aléo, J.-C. Ribierre, C. Adachi, *Chem. Mater.* **2018**, *30*, 6702.
- [35] V. T. N. Mai, V. Ahmad, M. Mamada, T. Fukunaga, A. Shukla, J. Sobus, G. Krishnan, E. G. Moore, G. G. Andersson, C. Adachi, E. B. Namdas, S.-C. Lo, *Nat. Commun.* **2020**, *11*, 5623.
- [36] M. Redecker, D. D. C. Bradley, M. Inbasekaran, E. P. Woo, *Appl. Phys. Lett.* **1998**, *73*, 1565.
- [37] V. G. Kozlov, G. Parthasarathy, P. E. Burrows, V. B. Khalfin, J. Wang, S. Y. Chou, S. R. Forrest, *IEEE J. Quantum Electron.* **2000**, *36*, 18.
- [38] a) Q. Zhang, L. Chi, G. Hai, Y. Fang, X. Li, R. Xia, W. Huang, E. Gu, *Molecules* **2017**, *22*, 315; b) H. Zhang, Q. Zhang, Q. Zhang, H. Sun, G. Hai, J. Tong, H. Xu, R. Xia, *Chin. Phys. B.* **2019**, *28*, 078108; c) Q. Niu, Q. Zhang, W. Xu, Y. Jiang, R. Xia, D. D. C. Bradley, D. Li, X. Wen, *Org. Electron.* **2015**, *18*, 95.
- [39] a) N. Tessler, N. T. Harrison, R. H. Friend, *Adv. Mater.* **1998**, *10*, 64; b) E. B. Namdas, P. Ledochowitsch, J. D. Yuen, D. Moses, A. J. Heeger, *Appl. Phys. Lett.* **2008**, *92*, 183304; c) T. Matsushima, H. Sasabe, C. Adachi, *Appl. Phys. Lett.* **2006**, *88*.
- [40] Q. Zhang, J. Liu, Q. Wei, X. Guo, Y. Xu, R. Xia, L. Xie, Y. Qian, C. Sun, L. Lüer, J. Cabanillas-Gonzalez, D. D. C. Bradley, W. Huang, *Adv. Funct. Mater.* **2018**, *28*, 1705824.
- [41] a) Y. Qian, Q. Wei, G. Del Pozo, M. M. Mroz, L. Lueer, S. Casado, J. Cabanillas-Gonzalez, Q. Zhang, L. Xie, R. Xia, W. Huang, *Adv. Mater.* **2014**, *26*, 2937; b) Q. Zhang, Y. Zhang, W. Xu, X. Li, J. Liu, X. Guo, R. Xia, W. Huang, *Opt. Express* **2015**, *23*, A465.
- [42] H. Nakanotani, H. Sasabe, C. Adachi, *Appl. Phys. Lett.* **2005**, *86*, 213506.
- [43] N. Koch, A. Kahn, J. Ghijsen, J. J. Pireaux, J. Schwartz, R. L. Johnson, A. Elschner, *Appl. Phys. Lett.* **2002**, *82*, 70.
- [44] a) P. Andrew, G. A. Turnbull, I. D. W. Samuel, W. L. Barnes, *Appl. Phys. Lett.* **2002**, *81*, 954; b) M. Reufer, S. Riechel, J. M. Lupton, J. Feldmann, U. Lemmer, D. Schneider, T. Benstem, T. Dobbertin, W. Kowalsky, A. Gombert, K. Forberich, V. Wittwer, U. Scherf, *Appl. Phys. Lett.* **2004**, *84*, 3262.
- [45] a) B. H. Wallikewitz, M. de la Rosa, J. H.-W. M. Kremer, D. Hertel, K. Meerholz, *Adv. Mater.* **2010**, *22*, 531; b) M. C. Gwinner, S. Khodabakhsh, M. H. Song, H. Schweizer, H. Giessen, H. Siringhaus, *Adv. Funct. Mater.* **2009**, *19*, 1360; c) T. Yamao, Y. Sakurai, K. Terasaki, Y. Shimizu, H. Jinnai, S. Hotta, *Adv. Mater.* **2010**, *22*, 3708; d) M. H. Song, D. Kabra, B. Wenger, R. H. Friend, H. J. Snaith, *Adv. Funct. Mater.* **2009**, *19*, 2130.
- [46] a) D. Pisignano, L. Persano, S. Gigli, P. Visconti, T. Stomeo, M. D. Vittorio, G. Barbarella, L. Favaretto, R. Cingolani, *Nanotechnology* **2004**, *15*, 766; b) M. G. Ramirez, P. G. Boj, V. Navarro-Fuster, I. Vragovic, J. M. Villalvilla, I. Alonso, V. Trabadelo, S. Merino, M. A. Díaz-García, *Opt. Express* **2011**, *19*, 22443; c) A. Seki, M. Ichikawa, N. Sugauma, Y. Tanaka, T. Koyama, Y. Taniguchi, *J. Photopolym. Sci. Technol.* **2003**, *16*, 329.
- [47] a) A. Genco, G. Giordano, S. Carallo, G. Accorsi, Y. Duan, S. Gambino, M. Mazzeo, *Org. Electron.* **2018**, *62*, 174; b) G. Canazza, F. Scotognella, G. Lanzani, S. De Silvestri, M. Zavelani-Rossi, D. Comoretto, *Laser Phys. Lett.* **2014**, *11*, 035804; c) M. Koschorreck, R. Gehlhaar, V. G. Lyssenko, M. Swoboda, M. Hoffmann, K. Leo, *Appl. Phys. Lett.* **2005**, *87*, 181108; d) B. Schuette, H. Gothe, S. I. Hintschich, M. Sudzius, H. Froeb, V. G. Lyssenko, K. Leo, *Appl. Phys. Lett.* **2008**, *92*, 163309.
- [48] X. Liu, H. Li, C. Song, Y. Liao, M. Tian, *Opt. Lett.* **2009**, *34*, 503.
- [49] a) T. Rabe, K. Gerlach, T. Riedl, H. H. Johannes, W. Kowalsky, J. Niederhofer, W. Gries, J. Wang, T. Weimann, P. Hinze, F. Galbrecht, U. Scherf, *Appl. Phys. Lett.* **2006**, *89*, 081115; b) H. Nakanotani, C. Adachi, S. Watanabe, R. Katoh, *Appl. Phys. Lett.* **2007**, *90*, 231109; c) Y. Zhang, S. R. Forrest, *Phys. Rev. B* **2011**, *84*, 241301; d) M. M. Mroz, G. Sforzini, Y. Zhong, K. S. Wong, H. L. Anderson, G. Lanzani, J. Cabanillas-Gonzalez, *Adv. Mater.* **2013**, *25*, 4347; e) A. S. D. Sandanayaka, K. Yoshida, M. Inoue, C. Qin, K. Goushi, J.-C. Ribierre, T. Matsushima, C. Adachi, *Adv. Opt. Mater.* **2016**, *4*, 834; f) A. S. D. Sandanayaka, K. Yoshida, M. Inoue, C. Qin, K. Goushi, J.-C. Ribierre, T. Matsushima, C. Adachi, *Adv. Opt. Mater.* **2016**, *4*, 809; g) A. S. D. Sandanayaka, L. Zhao, D. Pitrat, J.-C. Mulatier, T. Matsushima, C. Andraud, J.-H. Kim, J.-C. Ribierre, C. Adachi, *Appl. Phys. Lett.* **2016**, *108*, 223301.
- [50] D. Yokoyama, M. Moriwake, C. Adachi, *J. Appl. Phys.* **2008**, *103*, 123104.
- [51] Y. Han, L. Bai, M. Xu, X. An, C. Wei, L. Sun, N. Sun, M. Yu, H. Zhang, J. Lin, C. Ou, L. Xie, C. Yin, C. Sun, X. Ding, J. Cabanillas-Gonzalez, W. Huang, *Adv. Opt. Mater.* **2020**, *8*, 1902163.
- [52] a) Y. Zhao, L. Wang, X. Chen, B. Zhang, F. Shen, H. Song, H. Wang, *J. Mater. Chem. C* **2019**, *7*, 13447; b) I. McCulloch, M. Heeney, C. Bailey, K. Genevicius, I. MacDonald, M. Shkunov, D. Sparrowe, S. Tierney, R. Wagner, W. Zhang, M. L. Chabinyc, R. J. Kline, M. D. McGehee, M. F. Toney, *Nat. Mater.* **2006**, *5*, 328; c) J. Liu, H. Zhang, H. Dong, L. Meng, L. Jiang, L. Jiang, Y. Wang, J. Yu, Y. Sun, W. Hu, A. J. Heeger, *Nat. Commun.* **2015**, *6*, 10032; d) H.-H. Fang, R. Ding, S.-Y. Lu, J. Yang, X.-L. Zhang, R. Yang, J. Feng, Q.-D. Chen, J.-F. Song, H.-B. Sun, *Adv. Funct. Mater.* **2012**, *22*, 33; e) H. Wang, F. Li, I. Ravia, B. Gao, Y. Li, V. Medvedev, H. Sun, N. Tessler, Y. Ma, *Adv. Funct. Mater.* **2011**, *21*, 3770; f) X. Zhang, H. Dong, W. Hu, *Adv. Mater.* **2018**, *30*, 1801048.
- [53] Q. Ou, Q. Peng, Z. Shuai, *Nat. Commun.* **2020**, *11*, 4485.
- [54] E. Y. Choi, L. Mazur, L. Mager, M. Gwon, D. Pitrat, J. C. Mulatier, C. Monnerau, A. Fort, A. J. Attias, K. Dorkenoo, J. E. Kwon, Y. Xiao, K. Matczyszyn, M. Samoc, D. W. Kim, A. Nakao, B. Heinrich, D. Hashizume, M. Uchiyama, S. Y. Park, F. Mathevet, T. Aoyama, C. Andraud, J. W. Wu, A. Barsella, J. C. Ribierre, *Phys. Chem. Chem. Phys.* **2014**, *16*, 16941.
- [55] J.-C. Ribierre, L. Zhao, M. Inoue, P.-O. Schwartz, J.-H. Kim, K. Yoshida, A. S. D. Sandanayaka, H. Nakanotani, L. Mager, S. Méry, C. Adachi, *Chem. Commun.* **2016**, *52*, 3103.
- [56] J.-H. Kim, M. Inoue, L. Zhao, T. Komino, S. Seo, J.-C. Ribierre, C. Adachi, *Appl. Phys. Lett.* **2015**, *106*, 053302.
- [57] C.-C. Wu, Y.-T. Lin, K.-T. Wong, R.-T. Chen, Y.-Y. Chien, *Adv. Mater.* **2004**, *16*, 61.
- [58] T. Oyamada, C.-H. Chang, T.-C. Chao, F.-C. Fang, C.-C. Wu, K.-T. Wong, H. Sasabe, C. Adachi, *J. Phys. Chem. C* **2007**, *111*, 108.
- [59] H.-C. Cheng, Y.-H. Huang, H.-W. Lin, C.-H. Chang, K.-T. Wong, C.-H. Kuan, C.-C. Wu, *Org. Electron.* **2013**, *14*, 2540.
- [60] H. So, H. Watanabe, M. Yahiro, Y. Yang, Y. Oki, C. Adachi, *Opt. Mater.* **2011**, *33*, 755.
- [61] T. Spehr, R. Pudzich, T. Fuhrmann, J. Salbeck, *Org. Electron.* **2003**, *4*, 61.
- [62] T. Spehr, A. Siebert, T. Fuhrmann-Lieker, J. Salbeck, T. Rabe, T. Riedl, H. H. Johannes, W. Kowalsky, J. Wang, T. Weimann, P. Hinze, *Appl. Phys. Lett.* **2005**, *87*, 161103.
- [63] H. Nakanotani, S. Akiyama, D. Ohnishi, M. Moriwake, M. Yahiro, T. Yoshihara, S. Tobita, C. Adachi, *Adv. Funct. Mater.* **2007**, *17*, 2328.

- [64] C. C. Wu, M. C. DeLong, Z. V. Vardeny, J. P. Ferraris, *Synth. Met.* **2003**, 137, 939.
- [65] R. Kabe, H. Nakanotani, T. Sakanoue, M. Yahiro, C. Adachi, *Adv. Mater.* **2009**, 21, 4034.
- [66] a) H. Nakanotani, R. Kabe, M. Yahiro, T. Takenobu, Y. Iwasa, C. Adachi, *Appl. Phys. Express* **2008**, 1, 091801; b) H. Nakanotani, M. Saito, H. Nakamura, C. Adachi, *Appl. Phys. Lett.* **2009**, 95, 033308.
- [67] S. Varghese, S. K. Park, S. Casado, R. C. Fischer, R. Resel, B. Milián-Medina, R. Wannemacher, S. Y. Park, J. Gierschner, *J. Phys. Chem. Lett.* **2013**, 4, 1597.
- [68] Z. Xie, B. Yang, F. Li, G. Cheng, L. Liu, G. Yang, H. Xu, L. Ye, M. Hanif, S. Liu, D. Ma, Y. Ma, *J. Am. Chem. Soc.* **2005**, 127, 14152.
- [69] H. Wang, F. Li, B. Gao, Z. Xie, S. Liu, C. Wang, D. Hu, F. Shen, Y. Xu, H. Shang, Q. Chen, Y. Ma, H. Sun, *Cryst. Growth Des.* **2009**, 9, 4945.
- [70] a) S.-J. Yoon, S. Park, *J. Mater. Chem.* **2011**, 21, 8338; b) S.-J. Yoon, S. Varghese, S. K. Park, R. Wannemacher, J. Gierschner, S. Y. Park, *Adv. Opt. Mater.* **2013**, 1, 232.
- [71] S. Varghese, S.-J. Yoon, E. M. Calzado, S. Casado, P. G. Boj, M. A. Díaz-García, R. Resel, R. Fischer, B. Milián-Medina, R. Wannemacher, S. Y. Park, J. Gierschner, *Adv. Mater.* **2012**, 24, 6473.
- [72] S. Varghese, S.-J. Yoon, S. Casado, R. C. Fischer, R. Wannemacher, S. Y. Park, J. Gierschner, *Adv. Opt. Mater.* **2014**, 2, 542.
- [73] a) Q. Liao, X. Jin, H. Zhang, Z. Xu, J. Yao, H. Fu, *Angew. Chem., Int. Ed.* **2015**, 54, 7037; b) Z. Xu, Q. Liao, Q. Shi, H. Zhang, J. Yao, H. Fu, *Adv. Mater.* **2012**, 24, OP216.
- [74] W. Xie, Y. Li, F. Li, F. Shen, Y. Ma, *Appl. Phys. Lett.* **2007**, 90, 141110.
- [75] Y. Li, F. Shen, H. Wang, F. He, Z. Xie, H. Zhang, Z. Wang, L. Liu, F. Li, M. Hanif, L. Ye, Y. Ma, *Chem. Mater.* **2008**, 20, 7312.
- [76] H.-H. Fang, Q.-D. Chen, J. Yang, H. Xia, B.-R. Gao, J. Feng, Y.-G. Ma, H.-B. Sun, *J. Phys. Chem. C* **2010**, 114, 11958.
- [77] T. Aimono, Y. Kawamura, K. Goushi, H. Yamamoto, H. Sasabe, C. Adachi, *Appl. Phys. Lett.* **2005**, 86, 071110.
- [78] a) J.-M. Teng, Y.-F. Wang, C.-F. Chen, *J. Mater. Chem. C* **2020**, 8, 11340; b) S. Madayanad Suresh, D. Hall, D. Beljonne, Y. Olivier, E. Zysman-Colman, *Adv. Funct. Mater.* **2020**, 30, 1908677; c) Y. Liu, C. Li, Z. Ren, S. Yan, M. R. Bryce, *Nat. Rev. Mater.* **2018**, 3, 18020; d) Q. Zhang, B. Li, S. Huang, H. Nomura, H. Tanaka, C. Adachi, *Nat. Photonics* **2014**, 8, 326; e) X. Tang, L.-S. Cui, H.-C. Li, A. J. Gillett, F. Auras, Y.-K. Qu, C. Zhong, S. T. E. Jones, Z.-Q. Jiang, R. H. Friend, L.-S. Liao, *Nat. Mater.* **2020**, 19, 1332.
- [79] H. Uoyama, K. Goushi, K. Shizu, H. Nomura, C. Adachi, *Nature* **2012**, 492, 234.
- [80] H. Huang, Z. Yu, D. Zhou, S. Li, L. Fu, Y. Wu, C. Gu, Q. Liao, H. Fu, *ACS Photonics* **2019**, 6, 3208.
- [81] G. Tsiminis, N. A. Montgomery, A. L. Kanibolotsky, A. Ruseckas, I. F. Perepichka, P. J. Skabara, G. A. Turnbull, I. D. W. Samuel, *Semicond. Sci. Technol.* **2012**, 27, 094005.
- [82] G. Tsiminis, Y. Wang, P. E. Shaw, A. L. Kanibolotsky, I. F. Perepichka, M. D. Dawson, P. J. Skabara, G. A. Turnbull, I. D. W. Samuel, *Appl. Phys. Lett.* **2009**, 94, 243304.
- [83] R. Xia, W.-Y. Lai, P. A. Levermore, W. Huang, D. D. C. Bradley, *Adv. Funct. Mater.* **2009**, 19, 2844.
- [84] A. L. Kanibolotsky, F. Vilela, J. C. Forgie, S. E. T. Elmasly, P. J. Skabara, K. Zhang, B. Tiekke, J. McGurk, C. R. Belton, P. N. Stavrinou, D. D. C. Bradley, *Adv. Mater.* **2011**, 23, 2093.
- [85] Y. Wang, G. Tsiminis, Y. Yang, A. Ruseckas, A. L. Kanibolotsky, I. F. Perepichka, P. J. Skabara, G. A. Turnbull, I. D. W. Samuel, *Synth. Met.* **2010**, 160, 1397.
- [86] W. Xu, J. Yi, W.-Y. Lai, L. Zhao, Q. Zhang, W. Hu, X.-W. Zhang, Y. Jiang, L. Liu, W. Huang, *Adv. Funct. Mater.* **2015**, 25, 4617.
- [87] T. M. Figueira-Duarte, K. Müllen, *Chem. Rev.* **2011**, 111, 7260.
- [88] M. Uchimura, Y. Watanabe, F. Araoka, J. Watanabe, H. Takezoe, G.-I. Konishi, *Adv. Mater.* **2010**, 22, 4473.
- [89] a) R. D. Xia, G. Heliotis, D. D. C. Bradley, *Appl. Phys. Lett.* **2003**, 82, 3599; b) R. D. Xia, G. Heliotis, Y. B. Hou, D. D. C. Bradley, *Org. Electron.* **2003**, 4, 165; c) G. Heliotis, R. Xia, D. D. C. Bradley, G. A. Turnbull, I. D. W. Samuel, P. Andrew, W. L. Barnes, *Appl. Phys. Lett.* **2003**, 83, 2118; d) R. D. Xia, M. Campoy-Quiles, G. Heliotis, P. Stavrinou, K. S. Whitehead, D. D. C. Bradley, *Synth. Met.* **2005**, 155, 274; e) R. Xia, G. Heliotis, P. N. Stavrinou, D. D. C. Bradley, *Appl. Phys. Lett.* **2005**, 87; f) G. Ryu, R. Xia, D. D. C. Bradley, *J. Phys.: Condens. Matter* **2007**, 19, 056205.
- [90] a) M. Ariu, D. G. Lidzey, M. Sims, A. J. Cadby, P. A. Lane, D. D. C. Bradley, *J. Phys.: Condens. Matter* **2002**, 14, 9975; b) O. J. Korovyanko, Z. V. Vardeny, *Chem. Phys. Lett.* **2002**, 356, 361; c) P. E. Shaw, A. Ruseckas, J. Peet, G. C. Bazan, I. D. W. Samuel, *Adv. Funct. Mater.* **2010**, 20, 155; d) F. Montilla, A. Ruseckas, I. D. W. Samuel, *Chem. Phys. Lett.* **2013**, 585, 133.
- [91] a) M. Grell, D. D. C. Bradley, G. Ungar, J. Hill, K. S. Whitehead, *Macromolecules* **1999**, 32, 5810; b) A. J. Cadby, P. A. Lane, H. Mellor, S. J. Martin, M. Grell, C. Giebeler, D. D. C. Bradley, M. Wohlgenannt, C. An, Z. V. Vardeny, *Phys. Rev. B* **2000**, 62, 15604; c) G. Ryu, P. N. Stavrinou, D. D. C. Bradley, *Adv. Funct. Mater.* **2009**, 19, 3237; d) D. W. Bright, F. B. Dias, F. Galbrecht, U. Scherf, A. P. Monkman, *Adv. Funct. Mater.* **2009**, 19, 67; e) A. K. Bansal, A. Ruseckas, P. E. Shaw, I. D. W. Samuel, *J. Phys. Chem. C* **2010**, 114, 17864; f) H. J. Eggmann, F. Le Roux, L. M. Herz, *J. Phys. Chem. Lett.* **2019**, 10, 1729; g) A. Perevedentsev, Y. Sonnefraud, C. R. Belton, S. Sharma, A. E. G. Cass, S. A. Maier, J.-S. Kim, P. N. Stavrinou, D. D. C. Bradley, *Nat. Commun.* **2015**, 6, 5977.
- [92] C. Rothe, F. Galbrecht, U. Scherf, A. Monkman, *Adv. Mater.* **2006**, 18, 2137.
- [93] A. J. C. Kuehne, M. Kaiser, A. R. Mackintosh, B. H. Wallikewitz, D. Hertel, R. A. Pethrick, K. Meerholz, *Adv. Funct. Mater.* **2011**, 21, 2564.
- [94] Z. Yu, X. Guo, Q. Zhang, L. Chi, T. Chen, R. Xia, L. Wu, L. Luer, J. Cabanillas-Gonzalez, *J. Phys. Chem. C* **2016**, 120, 11350.
- [95] Y. Chen, J. Herrnsdorf, B. Guilhabert, A. L. Kanibolotsky, A. R. Mackintosh, Y. Wang, R. A. Pethrick, E. Gu, G. A. Turnbull, P. J. Skabara, I. D. W. Samuel, N. Laurand, M. D. Dawson, *Org. Electron.* **2011**, 12, 62.
- [96] A. Rose, Z. G. Zhu, C. F. Madigan, T. M. Swager, V. Bulovic, *Nature* **2005**, 434, 876.
- [97] E. B. Namdas, M. Tong, P. Ledochowitsch, S. R. Mednick, J. D. Yuen, D. Moses, A. J. Heeger, *Adv. Mater.* **2009**, 21, 799.
- [98] J. Y. Park, V. I. Srdanov, A. J. Heeger, C. H. Lee, Y. W. Park, *Synth. Met.* **1999**, 106, 35.
- [99] A. E. Vasdekis, G. A. Turnbull, I. D. W. Samuel, P. Andrew, W. L. Barnes, *Appl. Phys. Lett.* **2005**, 86, 161102.
- [100] G. A. Turnbull, P. Andrew, W. L. Barnes, I. D. W. Samuel, *Appl. Phys. Lett.* **2003**, 82, 313.
- [101] I. B. Martini, I. M. Craig, W. C. Molenkamp, H. Miyata, S. H. Tolbert, B. J. Schwartz, *Nat. Nanotechnol.* **2007**, 2, 647.
- [102] a) M. S. AlSalhi, K. H. Ibaouf, V. Masilamani, O. A. Yassin, *J. Lumin.* **2012**, 132, 484; b) G. Yang, X. Chen, Y. Wang, S. Feng, *Opt. Express* **2013**, 21, 11457.
- [103] U. Scherf, K. Müllen, *Makromol. Chem., Rapid Commun.* **1991**, 12, 489.
- [104] A. C. Grimsdale, K. Müllen, *Macromol. Rapid Commun.* **2007**, 28, 1676.
- [105] J. D. Plumbhof, T. Stoefler, L. Mai, U. Scherf, R. F. Mahrt, *Nat. Mater.* **2014**, 13, 248.

- [106] C. Kallinger, M. Hilmer, A. Haugeneder, M. Perner, W. Spirkl, U. Lemmer, J. Feldmann, U. Scherf, K. Mullen, A. Gombert, V. Wittwer, *Adv. Mater.* **1998**, *10*, 920.
- [107] F. Laquai, A. K. Mishra, M. R. Ribas, A. Petrozza, J. Jacob, L. Akcelrud, K. Müllen, R. H. Friend, G. Wegner, *Adv. Funct. Mater.* **2007**, *17*, 3231.
- [108] F. Laquai, A. K. Mishra, K. Müllen, R. H. Friend, *Adv. Funct. Mater.* **2008**, *18*, 3265.
- [109] H. Kim, N. Schulte, G. Zhou, K. Müllen, F. Laquai, *Adv. Mater.* **2011**, *23*, 894.
- [110] a) M. Berggren, A. Dodabalapur, R. E. Slusher, Z. Bao, *Synth. Met.* **1997**, *91*, 65; b) V. G. Kozlov, V. Bulovic, P. E. Burrows, M. Baldo, V. B. Khalfin, G. Parthasarathy, S. R. Forrest, Y. You, M. E. Thompson, *J. Appl. Phys.* **1998**, *84*, 4096.
- [111] a) R. Xia, P. N. Stavrinou, D. D. C. Bradley, Y. Kim, *J. Appl. Phys.* **2012**, *111*, 123107; b) L. Wu, S. Casado, B. Romero, J. M. Oton, J. Morgado, C. Mueller, R. Xia, J. Cabanillas-Gonzalez, *Macromolecules* **2015**, *48*, 8765.
- [112] L. Wu, F. Luo, L. Luer, B. Romero, J. M. Oton, Q. Zhang, R. Xia, J. Cabanillas-Gonzalez, *J. Polym. Sci. Part B: Polym. Phys.* **2016**, *54*, 2311.
- [113] Y. Xu, G. Hai, H. Xu, H. Zhang, Z. Zuo, Q. Zhang, R. Xia, C. Sun, J. Castro-Smirnov, A. Sousaraei, S. Casado, M. R. Osorio, D. Granados, I. Rodriguez, J. Cabanillas-Gonzalez, *Adv. Opt. Mater.* **2018**, *6*, 1800263.
- [114] a) J. Hill, S. Y. Heriot, O. Worsfold, T. H. Richardson, A. M. Fox, D. D. C. Bradley, *Synth. Met.* **2003**, *139*, 787; b) J. Chappell, D. G. Lidzey, P. C. Jukes, A. M. Higgins, R. L. Thompson, S. O'Connor, I. Grizzi, R. Fletcher, J. O'Brien, M. Geoghegan, R. A. L. Jones, *Nat. Mater.* **2003**, *2*, 616; c) S. Lattante, A. Cretí, M. Lomascolo, M. Anni, *Org. Electron.* **2016**, *29*, 44; d) C. R. McNeill, N. C. Greenham, *Adv. Mater.* **2009**, *21*, 3840.
- [115] A. R. Buckley, M. D. Rahn, J. Hill, J. Cabanillas-Gonzalez, A. M. Fox, D. D. C. Bradley, *Chem. Phys. Lett.* **2001**, *339*, 331.
- [116] a) R. Brückner, A. A. Zakhidov, R. Scholz, M. Sudzius, S. I. Hintschich, H. Fröb, V. G. Lyssenko, K. Leo, *Nat. Photonics* **2012**, *6*, 322; b) A. Mischok, R. Brückner, M. Sudzius, C. Reinhardt, V. G. Lyssenko, H. Fröb, K. Leo, *Appl. Phys. Lett.* **2014**, *105*, 051108; c) M. Sudzius, M. Langner, S. I. Hintschich, V. G. Lyssenko, H. Fröb, K. Leo, *Appl. Phys. Lett.* **2009**, *94*, 061102.
- [117] K. Yamashita, T. Nakahata, T. Hayakawa, Y. Sakurai, T. Yamao, H. Yanagi, S. Hotta, *Appl. Phys. Lett.* **2014**, *104*, 253301.
- [118] P. Lova, V. Grande, G. Manfredi, M. Patrini, S. Herbst, F. Würthner, D. Comoretto, *Adv. Optical Mater.* **2017**, *5*, 1700523.
- [119] G. Canazza, F. Scotognella, G. Lanzani, S. De Silvestri, M. Zavelani-Rossi, D. Comoretto, *Laser Phys. Lett.* **2014**, *11*, 3.
- [120] a) M. Chakaroun, A. Coens, N. Fabre, F. Gourdon, J. Solard, A. Fischer, A. Boudrioua, C. C. Lee, *Opt. Express* **2011**, *19*, 493; b) A. Coens, M. Chakaroun, A. P. A. Fischer, M. W. Lee, A. Boudrioua, B. Geffroy, G. Vemuri, *Opt. Express* **2012**, *20*, 29252.
- [121] J. Lin, Y. Hu, Y. Lv, X. Guo, X. Liu, *Sci. Bull.* **2017**, *62*, 1637.
- [122] M. Wang, J. Lin, Y.-C. Hsiao, X. Liu, B. Hu, *Nat. Commun.* **2019**, *10*, 1614.
- [123] J. Lin, Y. Hu, X. Liu, *Adv. Opt. Mater.* **2020**, *8*, 1901421.
- [124] a) H. Kogelnik, C. V. Shank, *J. Appl. Phys.* **1972**, *43*, 2327; b) H. Kogelnik, C. V. Shank, *Appl. Phys. Lett.* **1971**, *18*, 152.
- [125] a) A. E. Vasdekis, G. Tsiminis, J. C. Ribierre, L. O'Faolain, T. F. Krauss, G. A. Turnbull, I. D. W. Samuel, *Opt. Express* **2006**, *14*, 9211; b) H. Sakata, H. Takeuchi, *Appl. Phys. Lett.* **2008**, *92*, 113310.
- [126] a) J. R. C. Smirnov, A. Sousaraei, M. R. Osorio, S. Casado, J. J. Hernández, L. Wu, Q. Zhang, R. Xia, D. Granados, R. Wannemacher, I. Rodriguez, J. Cabanillas-Gonzalez, *npj Flex. Electron.* **2019**, *3*, 17; b) D. Sanchez-deAlcazar, D. Romera, J. Castro-Smirnov, A. Sousaraei, S. Casado, A. Espasa, M. C. Morant-Miñana, J. J. Hernandez, I. Rodríguez, R. D. Costa, J. Cabanillas-Gonzalez, R. V. Martinez, A. L. Cortajarena, *Nanoscale Adv.* **2019**, *1*, 3980.
- [127] a) M. G. Ramirez, P. G. Boj, V. Navarro-Fuster, I. Vragovic, J. M. Villalvilla, I. Alonso, V. Trabadelo, S. Merino, M. A. Diaz-Garcia, *Opt. Express* **2011**, *19*, 22443; b) D. Pisignano, L. Persano, P. Visconti, R. Cingolani, G. Gigli, G. Barbarella, L. Favaretto, *Appl. Phys. Lett.* **2003**, *83*, 2545.
- [128] T. Zhai, F. Cao, S. Chu, Q. Gong, X. Zhang, *Opt. Express* **2018**, *26*, 4491.
- [129] a) P. Görrn, M. Lehnhardt, W. Kowalsky, T. Riedl, S. Wagner, *Adv. Mater.* **2011**, *23*, 869; b) A. Berdin, H. Rekola, O. Sakhno, M. Wegener, A. Priimagi, *Opt. Express* **2019**, *27*, 25634.
- [130] M. Stroisch, T. Woggon, C. Teiwes-Morin, S. Klinkhammer, K. Forberich, A. Gombert, M. Gerken, U. Lemmer, *Opt. Express* **2010**, *18*, 5890.
- [131] a) K. Baumann, T. Stöferle, N. Moll, R. F. Mahrt, T. Wahlbrink, J. Bolten, T. Mollenhauer, C. Moormann, U. Scherf, *Appl. Phys. Lett.* **2007**, *91*, 171108; b) K. Baumann, T. Stöferle, N. Moll, G. Raino, R. F. Mahrt, T. Wahlbrink, J. Bolten, U. Scherf, *J. Opt.* **2010**, *12*, 065003; c) G. Heliotis, R. Xia, D. D. C. Bradley, G. A. Turnbull, I. D. W. Samuel, P. Andrew, W. L. Barnes, *J. Appl. Phys.* **2004**, *96*, 6959; d) G. Heliotis, R. D. Xia, G. A. Turnbull, P. Andrew, W. L. Barnes, I. D. W. Samuel, D. D. C. Bradley, *Adv. Funct. Mater.* **2004**, *14*, 91; e) G. A. Turnbull, P. Andrew, W. L. Barnes, I. D. W. Samuel, *Phys. Rev. B* **2003**, *67*, 165107.
- [132] E. M. Calzado, A. Retolaza, S. Merino, M. Morales-Vidal, P. G. Boj, J. A. Quintana, J. M. Villalvilla, M. A. Díaz-García, *Opt. Mater. Express* **2017**, *7*, 1295.
- [133] S. Zhang, L. B. Cui, X. Zhang, J. H. Tong, T. R. Zhai, *Opt. Express* **2020**, *28*, 2809.
- [134] K. Yoshino, S. Tatsuhara, Y. Kawagishi, M. Ozaki, A. A. Zakhidov, Z. V. Vardeny, *Appl. Phys. Lett.* **1999**, *74*, 2590.
- [135] a) Y. Nishijima, K. Ueno, S. Juodkakis, V. Mizeikis, H. Misawa, M. Maeda, M. Minaki, *Opt. Express* **2008**, *16*, 13676; b) F. Castles, F. V. Day, S. M. Morris, D. H. Ko, D. J. Gardiner, M. M. Qasim, S. Nosheen, P. J. W. Hands, S. S. Choi, R. H. Friend, H. J. Coles, *Nat. Mater.* **2012**, *11*, 599.
- [136] V. Ahmad, J. Sobus, M. Greenberg, A. Shukla, B. Philippa, A. Pivrikas, G. Vamvounis, R. White, S.-C. Lo, E. B. Namdas, *Nat. Commun.* **2020**, *11*, 4310.
- [137] I. S. Grudinina, V. S. Ilchenko, L. Maleki, *Phys. Rev. A* **2006**, *74*, 063806.
- [138] S. Klinkhammer, T. Grossmann, K. Lüll, M. Hauser, C. Vannahme, T. Mappes, H. Kalt, U. Lemmer, *IEEE Photonics Technol. Lett.* **2011**, *23*, 489.
- [139] X. Lu, X. Wang, Q. Liao, H. Fu, *J. Phys. Chem. C* **2015**, *119*, 22108.
- [140] S. K. Y. Tang, Z. Li, A. R. Abate, J. J. Agresti, D. A. Weitz, D. Psaltis, G. M. Whitesides, *Lab. Chip* **2009**, *9*, 2767.
- [141] Y. Wang, H. Li, L. Zhao, Y. Liu, S. Liu, J. Yang, *Appl. Phys. Lett.* **2016**, *109*, 231906.
- [142] A. François, N. Riesen, H. Ji, S. Afshar, T. M. Monro, *Appl. Phys. Lett.* **2015**, *106*, 031104.
- [143] A. François, M. Himmelfhaus, *Appl. Phys. Lett.* **2009**, *94*, 031101.
- [144] D. Okada, Z.-H. Lin, J.-S. Huang, O. Oki, M. Morimoto, X. Liu, T. Minari, S. Ishii, T. Nagao, M. Irie, Y. Yamamoto, *Mater. Horizons* **2020**, *7*, 1801.
- [145] Z. Gao, C. Wei, Y. Yan, W. Zhang, H. Dong, J. Zhao, J. Yi, C. Zhang, Y. J. Li, Y. S. Zhao, *Adv. Mater.* **2017**, *29*, 1701558.

- [146] S. V. Frolov, Z. V. Vardeny, K. Yoshino, A. Zakhidov, R. H. Baughman, *Phys. Rev. B* **1999**, 59, R5284.
- [147] L. B. Bai, C. Sun, Y. M. Han, C. X. Wei, X. An, L. L. Sun, N. Sun, M. N. Yu, K. N. Zhang, J. Y. Lin, M. Xu, L. H. Xie, H. F. Ling, J. Cabanillas-Gonzalez, L. Song, X. T. Hao, W. Huang, *Adv. Opt. Mater.* **2020**, 8, 8.
- [148] M. Anni, D. Rhee, W.-K. Lee, *ACS Appl. Mat. Interfaces* **2019**, 11, 9385.
- [149] A. Sarkar, N. N. S. Ojha, B. N. S. Bhaktha, *Appl. Phys. Lett.* **2017**, 110, 251104.
- [150] Y.-J. Lee, C.-Y. Chou, Z.-P. Yang, T. B. H. Nguyen, Y.-C. Yao, T.-W. Yeh, M.-T. Tsai, H.-C. Kuo, *Nanoscale* **2018**, 10, 10403.
- [151] X. Li, H. Liu, X. Xu, B. Yang, H. Yuan, J. Guo, F. Sang, Y. Jin, *ACS Appl. Mat. Interfaces* **2020**, 12, 10050.
- [152] Y.-J. Lee, T.-W. Yeh, Z.-P. Yang, Y.-C. Yao, C.-Y. Chang, M.-T. Tsai, J.-K. Sheu, *Nanoscale* **2019**, 11, 3534.
- [153] V. D. Ta, D. Saxena, S. Caixeiro, R. Sapienza, *Nanoscale* **2020**, 12, 12357.
- [154] B. Xu, Z. Gao, Y. Wei, Y. Liu, X. Sun, W. Zhang, X. Wang, Z. Wang, X. Meng, *Nanoscale* **2020**, 12, 4833.
- [155] Y.-T. Hsu, Y.-Y. Lin, Y.-Z. Chen, H.-Y. Lin, Y.-M. Liao, C.-F. Hou, M.-H. Wu, W.-N. Deng, Y.-F. Chen, *Adv. Mater. Technol.* **2020**, 5, 1900742.
- [156] M. Umar, K. Min, S. Kim, S. Kim, *Sci. Rep.* **2019**, 9, 16266.
- [157] S. Kéna-Cohen, S. R. Forrest, *Nat. Photonics* **2010**, 4, 371.
- [158] D. G. Lidzey, D. D. C. Bradley, M. S. Skolnick, T. Virgili, S. Walker, D. M. Whittaker, *Nature* **1998**, 395, 53.
- [159] K. S. Daskalakis, S. A. Maier, R. Murray, S. Kéna-Cohen, *Nat. Mater.* **2014**, 13, 271.
- [160] J. D. Plumhof, T. Stöferle, L. Mai, U. Scherf, R. F. Mahrt, *Nat. Mater.* **2014**, 13, 247.
- [161] M. Wei, S. K. Rajendran, H. Ohadi, L. Tropic, M. C. Gather, G. A. Turnbull, I. D. W. Samuel, *Optica* **2019**, 6, 1124.
- [162] S. K. Rajendran, M. Wei, H. Ohadi, A. Ruseckas, G. A. Turnbull, I. D. W. Samuel, *Adv. Opt. Mater.* **2019**, 7, 1801791.
- [163] Y. Qu, S. Hou, S. R. Forrest, *ACS Photonics* **2020**, 7, 867.
- [164] A. Putintsev, A. Zasedatelev, K. E. McGhee, T. Cookson, K. Georgiou, D. Sannikov, D. G. Lidzey, P. G. Lagoudakis, *Appl. Phys. Lett.* **2020**, 117, 123302.



Qi Zhang received his Ph.D. in electronic science and engineering in 2017 from Nanjing University of Posts and Telecommunications under the supervision of Professor Wei Huang (member of Chinese Academy of Science). After that, he worked as a postdoctoral researcher in IMDEA Nanociencia focusing on organic photophysics. Now, he is working with Professor Donal Bradley (fellow of the Royal Society) as a postdoctoral researcher of King Abdullah University of Science and Technology. His research interests include photophysics of organic/inorganic semiconductors, device physics, and nanofabrication.



Wenwen Tao received her master's degree from Soochow University, majoring in materials science and engineering. Currently, she is a research technician in Oxford Suzhou Centre for Advanced Research. Her research interest focuses on fully solution-processable organic light-emitting devices.



Jingsong Huang is Head of Optoelectronic Technology Laboratory, Oxford Suzhou Center for Advanced Research. He received a Ph.D. in State Key Laboratory on Integrated Optoelectronics, Jilin University, in 2000. He was a research fellow of Alexander von Humboldt Foundation. He is a guest professor of South China University of Technology. He has a 20-year track record of research activities in leading universities and industries. His specialty is organic semiconducting materials and devices, especially in the application research of photovoltaics and light-emitting diodes.



Ruidong Xia is the Deputy Head of the International School of Advanced Materials, South China University of Technology. She received a Ph.D. in electrical and electronic engineering in University of Nottingham, UK. She joined Plastic Electronic Center, Imperial College London, in 2002. She was appointed as professor in optoelectronics at Nanjing University of Post and Telecommunication in 2012. Her research interests have been focused on molecular optoelectronic materials and devices including polymer lasers, optical amplifiers, light-emitting diodes, and solar cells. Her works have led to over 100 publications.



Juan Cabanillas-Gonzalez is Head of the Organic Photophysics and Photonics group at IMDEA Nanociencia (Spain). He received a Ph.D. in physics from Imperial College London, working with photophysics of conjugated polymers with Professor Donal Bradley. Following a postdoctoral position at Politecnico di Milano, he was subsequently appointed Ramon y Cajal research fellow and research professor at IMDEA Nanociencia. His main research interests concern femtosecond spectroscopy, solution-processed semiconductors, and optoelectronic applications.